Functionalized nanodiamonds as a perspective green carbo-catalyst for removal of emerging organic pollutants

Robert Bogdanowicz*

Department of Metrology and Optoelectronics, Faculty of Electronics, Telecommunications and Informatics, Gdańsk University of Technology, 11/12 Gabriela Narutowicza Street, 80-233 Gdańsk, Poland

* tel. +4858 347 1503, email: rbogdan@eti.pg.edu.pl (*R. Bogdanowicz*)

Abstract. Rapid industrial and urban development jointly with rising global population strongly affect the large-scale issues with drinking, groundwater, and surface water pollution. Concerns are not limited to environmental issues but also human health impact becoming serious global aspect. Organic pollution becomes a primarily serious hazard, therefore, the novel sophisticated approaches to treat them are thoroughly investigated. Among numerous materials, functionalized nanodiamonds are specific versatile nanocarbon material attracted ample attention thanks to their exceptional chemical, optical and electronic properties beneficial in the decomposition of harmful organic chemicals.

This work delivers a comprehensive review of progress and perspectives on the green-friendly nanodiamonds, which are suitable for the degradation of emerging organic pollutants using numerous approaches utilizing them as an electro-oxidation catalyst; photocatalyst; oxidation agent, or adsorbing surface. Novel modification strategies of nanodiamonds (*i.e.*, persulfates, oxides, or metals) remarkably improve pollutant removal efficiency and facilitate charge transfer and surface regeneration. Furthermore, we evaluated also the influence of various factors like pH, natural organic matters, or radical scavengers on the removal efficiency combining them with nanodiamond properties. The identified missing research gaps and development perspectives of nanodiamond surfaces in water remediation relating to other nanocarbon and metal catalysts were also here described.

Keywords: nanodiamond, carbo-catalyst, metal-free catalyst, electro-oxidation, photocatalytic oxidation, organic pollutants removal.

1. Introduction

The multifunctional behaviour of small diamond particles called nanodiamonds (ND) attracts different researchers [1] due to their unique parameters useful in biotechnology [2,3], batteries [4], electronics [5], quantum or environmental applications [3]. Thanks to the exceptional sp^3 hybridized, tetrahedral bonds, nanodiamond outperform other nanocarbons since they could be scaled from close to zero-dimensional to three-dimensional (3D) particles with flexible surficial terminations resulting in remarkable physicochemical performance [6]. The hardness, wearability, good chemical stability of NDs have been regarded as some of

the most useful materials in modern applications [7,8]. Various routines were already established to fabricate single crystal, high-quality nanodiamonds including high-pressure high temperature (HPHT) or synthesis of large amounts of nanodiamond particles by the explosion. Detonation nanodiamonds (DND) were recognized as a sustainable environmental and metal-free material, which is non-toxic and relatively low-cost versus other nanocarbons. The wide-ranging HPHT nanodiamond diameters could be achieved by high-energy ball milling, where crystals are broken without amorphization [9]. HPHT NDs are purely made of cubic C-diamond nanocrystals with specific diameters and high crystallinity [10]. They lack a non-diamond shell exhibiting low level of impurities as manifested by Stehlik *et al.* [2]. DNDs are rich in *sp²* shell being mostly useful for various applications not only limited to the typical wear applications [11]. Next, milling or sonication process could be utilized to achieve a quasi-spherical aqueous colloidal dispersion of nanoparticles [12]. The *sp²* carbon shell of DNDs could be modified to alternate their properties towards different functions including also catalysis and photocatalysis as well as electrodes with moderately high specific surface areas about 260 m^2/g and nano-porosity [13]. Surface performance of ND particles could be modified by various termination involving hydrogen, hydroxyl, ester, carboxyl, carbonyl or ether groups, which allows to adjust their reactivity.
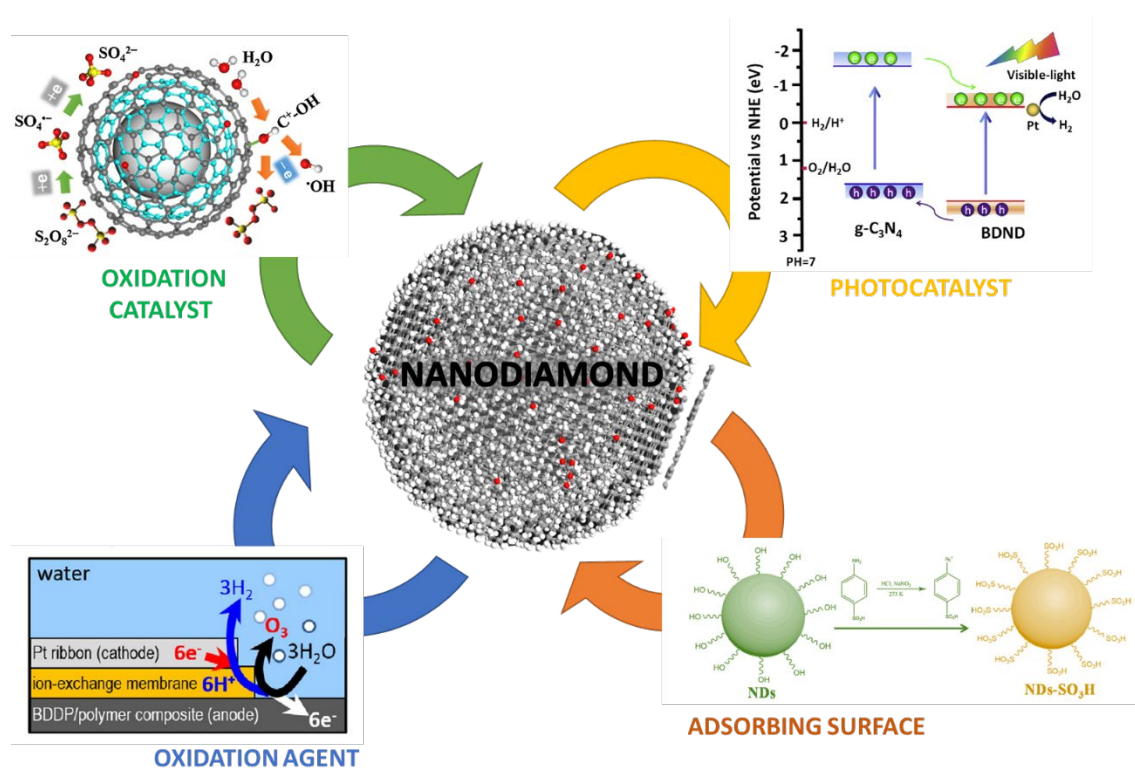
Figure 1. Schematic diagram representing main approaches of nanodiamond application for degradation of emerging organic pollutants. Reproduced with permission from following Refs. [14] reporting nanodiamond as electro-oxidation catalyst; [15] photocatalyst; [16] oxidation agent and [17] adsorbing surface.

Rapid urbanization and industrialization along with global population rise affect the large-scale issues with water pollutants including drinking, groundwater, and surface water sources. It is not just limited to environmental concerns but also human health impact becoming a serious global issue [18]. The emerging

2

organic pollutants commonly detected in water include pharmaceuticals, endocrine disruptors, pesticides, dyes, detergents, or widespread industrial organic wastes (*i.e.*, phenols, halogens, and aromatic compounds). The increasing spread of organic pollution becomes a serious hazard to the world health and environment, therefore, the development of novel sophisticated approaches to treat them are thoroughly investigated.

The novel strategies of catalytic removal of emerging organic pollutants are extremely demanded, thus versatile nanodiamonds (NDs) are specific nano-carbon materials that attracted ample attention thanks to their exceptional chemical, optical and electronic properties useful in the decomposition of harmful organic chemicals. Lately, the diamond composites become an attractive novel materials combine the properties of continuous diamond films along with single ND particles advances. Such an approach plays a crucial for time-stable and low ecotoxic photo- and electro-catalytic applications [19,20]. Up to date, a few important works have been published reviewing applications of NDs in biotechnology, photonics, electronics, and catalysis [18,21,22]. The last ones are focused on the various catalytic processes revealing structural and chemical properties of NDs that have led to the enhanced catalytic activity [13] confronted with other carbon allotropes.

In this review, we report for the first time the recent progress on the green-oriented NDs applications in degradation of emerging organic pollutants using numerous approaches utilizing them as electro-oxidation catalyst [14]; photocatalyst [15]; oxidation agent [16], or adsorbing surface [17] (see Figure 1). Moreover, we reviewed also the influence of various factors like pH, natural organic matters, or radical scavengers on the removal efficiency, combining them with ND properties along with their fabrication followed by surface modification.

2. Graphitized Nanodiamonds for Removal of Organic Compounds by oxidation: a metal-free carbo-catalyst

Graphitized nanodiamond shows a unique catalytic effect being a kind of recent metal-free catalysis [14,23]. ND surface graphitization of NDs was achieved by thermal annealing forming surficial sp^2 hybridized shell. Such an approach allows for activation by persulfates (PS) delivering extended catalytic performance toward wastewater remediation and pollutants treatment. Results shown in that section were conducted revealing the impact of various parameters as pH, temperature, ND loading, PS addition or concentration of pollutant (mostly phenols) as well as the interfering agents like chlorine ions or humic acid (see Table 1). The crucial role in catalytic processes plays functional groups and defective sites at NDs inducing superoxides activation. PS/ND complex showed slightly improved control of oxidation processes relating to metal-based systems [18].

Duan *et al.* [14] demonstrated that annealed nanodiamonds are capable to activate persulfates generating hydroxyl radicals (•OH) and sulfate radicals (SO_4•$^-$), induced by water molecules oxidation at the graphitized nanodiamond surface (see Figure 1 or 4A). NDs were annealed at temperatures of 600–1000∘C under N_2

(AND-X (X = 600, 700, 800, 900, and 1000) to achieve a superb tunnel for charge transfer. Those systems presented 75.4% of phenol removal at 15◦C in just 120 min. The full phenol oxidation was achieved using AND-1000 at 25◦C after 45 minutes. Furthermore, an analogous phenomenon was investigated by Lee *et al.* [24] manifesting total phenol removal in10 min (see Figure 2A) on graphitized ND in comparison to bare ND with peroxydisulfate (PDS) which removed barely 25% of phenol in 1 hour. Moreover, oxygen terminated ND/PDS did not induce phenol oxidation. Graphitized ND (G-ND) results in a comparable cluster diameter to bare NDs, while they showed onion-like core-shell composition consisting of multi-graphitic sp^2 layers similarly to vertical graphene-diamond nanostructures [25,26]. Inset in Figure 2A displays HR-TEM image of G-NDs clusters with an average size of 185 ± 10 nm attained in aqueous media. Reported studies raised wider public debate on the reached efficiency and its mechanistic origin [27,28].

It is worth noting that G-ND treated at elevated temperatures manifests improved phenol removal supported by PDS admixture (see Figure 2B). It was stated that the sp^2 shell of ND induced PDS activation. The lower oxygen concentration at the ND surface displays an enhanced catalytic effect. Moreover, the phenol removal rate tends to grow with larger G-ND loading and decreasing versus initial phenol concentration [24].
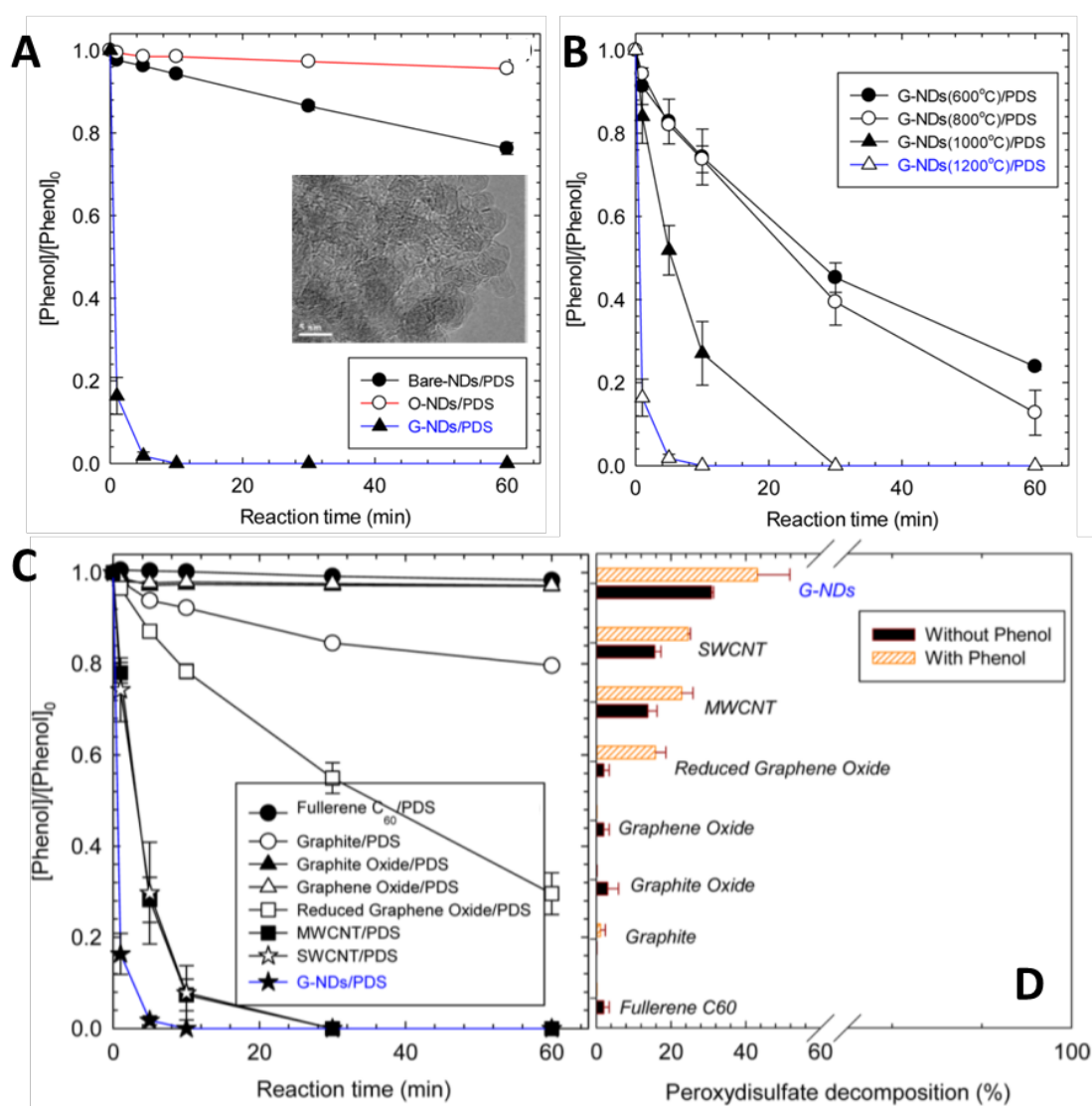
Figure 2. (A) Time-resolved phenol removal at surface-modified NDs (Inset: HR-TEM images of graphitized ND samples) and (B) graphitized ND annealed at different temperatures in the presence of peroxydisulfate (PDS), (C, D) Phenol removal by carbon-materials removal of peroxydisulfate (PDS). Reproduced with permission from Ref. [24]. Copyright 2016, American Chemical Society.

Figures 2CD display that G-ND outperforms other nanocarbon materials like graphite, graphene, fullerene or carbon nanotubes resulting in superb persulfate activation [24]. Combined G-ND and PDS presence improved phenol removal with the first-order rate constants, k =0.846 ± 0.132 min^{-1}. The various carbon nanotubes (CNT) showed comparable but still lower than G-ND rates of PDS decomposition (see Figure 4D). A remarkable rate of PDS decomposition was observed for both G-NDs and CNTs with phenol admixture, which serving as a donor of electrons to increase the kinetics of PDS decomposition processes.

These findings suggest that mostly radical intermediates (sulfate radical anion, hydroxyl radical) are driving the oxidation of organic pollutants supported by PDS. Nevertheless, G-ND performs a crucial role (literally sp^2 phase) in facilitating charge transfer from phenol to persulfate. Detailed studies of Shao *et al.* [29] manifested that annealing of ND formed ketonic carbonyl groups, which are primarily catalytically active sites. They summarized that ND - peroxymonosulfate (PMS) system manifest high $^1O_2$ selectivity outperformed the standard radical-induced oxidation processes during organic pollutants mineralization in aqueous media.

Figure 3A displays EPR spectra annealed at various temperatures compared to pristine NDs S-ND-X (X = 500–1000). EPR revealed that thermal treatment significantly decreases the intensity and levels of paramagnetic centres. This effect is attributed to sp^2 structural defects (dangling bonds, vacancies, and edging sites) created at the diamond core (lattice spacing of diamond [001], 0.204 nm), which is thermally decomposed decreasing its size as shown also in the HRTEM image (Inset of Figure 3A). The number of graphitic layers increased in the onion-like shell for larger temperature resulting also in reduced size of the diamond core of 2∼ 3 nm is presented in Figure 3A. Moreover, the nanodiamond graphitization grade was detected by the electron energy loss spectroscopy (EELS) in Duan *et al.* work [30] and applied for enhanced degradation of phenol by activating persulfate. The synergistic interactions of sp^2 and sp^3 phases are responsible for electron transfer from the nanodiamond core to the outer shell, improving the O-O fragmentation.

Duan *et al.* [30] demonstrated also a strong covalent bonding of graphene shell with the diamond core using DFT simulations (see Figure 3B). It was also shown that other top graphene flakes on diamond interact with other sp^2 layers by the van der Waals weak interfaces. The peroxymonosulfate (PMS) molecule tends to position at the outer graphene flake regardless number of graphitic layers in the shells. Simulations also revealed saturation of charge transfer from graphene to PMS for more graphitic layers resulting in lower electron densities, which also observed as decreased kinetics of phenol degradation for nanodiamond annealed

at 1100ºC displayed in Figure 3D. The DFT results imply also that the enhanced electrical conductivity induced by graphitization induces higher activation of persulfates.

The catalytic performance towards phenol degradation was improved considerably for nanodiamond annealed at 900°C (attn. Figure 3C) when compared to pristine diamonds. Obviously, the graphitization process and further catalytic effect depend also strongly on the nanodiamond structure induced by fabrication used by the specific supplier (I-ND (Ray Techniques Ltd., Israel), C-ND (XFnano Materials Tech Co. Ltd., China), and S-ND Sigma-Aldrich, Australia). Both DFT simulations and XPS studies of annealed nanodiamond surface revealed that thermal treatment in atmosphere causes defects inducing efficient graphitization and thus increased conductivity [31]. The formed in that process ketonic carbonyl groups were attributed as the main catalytic sites responsible for activation of peroxymonosulfate [29]. Furthermore, it was shown that the most reactive oxygen species in PMS/ND system are singlet oxygens enabling enhanced selectivity of target pollutant oxidation.
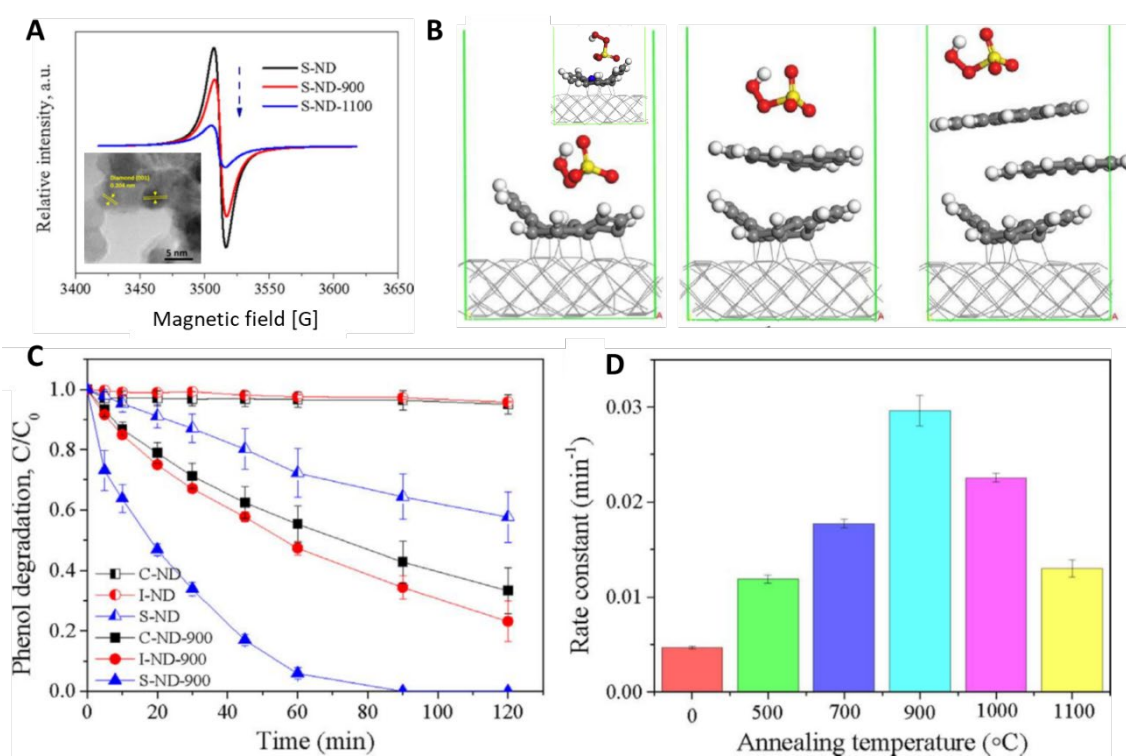

Figure 3. (A) Electron resonance and TEM image of nanodiamond particles annealed at different temperatures, (B) slabs of relaxed peroxymonosulfate adsorbed at on graphene/diamond system with a different number of layers (Inset: nitrogen-doped graphene with peroxymonosulfate), (C) Phenol degradation using bare and graphitized nanodiamonds; (D) influence of annealing temperature on the catalytic performance of detonation nanodiamond. Reproduced with permission from Ref. [30]. Copyright 2017, Elsevier.

All the thermally treated nanodiamonds revealed enhanced catalytic effect, while their organic removal rates differ by over 40%. The use of PMS jointly with C-ND-900 and I-ND-900 achieved 66.7% and 76.9% phenol degradation in 120 min, while the smallest and deagglomerated particles S-ND-900 allowed for total phenol degradation in just 90 min. The smallest crystals undergo a more efficient graphitization process, thus, exhibits larger specific surfaces area and higher surface energy resulting in the improved activity of nanodiamond

6

complexes. Organic pollutants treatment (*i.e.*, phenol oxidation) efficiency is significantly tuned by the thermal treatment as shown in Figure 3D. This effect is attributed to the energetic optimization of graphitized nanodiamond surface and its reconstruction.

Most recently, Yang *et al.* [23] demonstrated that thermally treated nanodiamonds elevated temperatures of 2000°C (ND-2000) outperformed prior works thanks to rapidly improved and specifically driven sp^3 to sp^2 reconstruction of the inner diamond core and decomposition of its outer shell. They reported also that photoirradiation of ND/PDS system causes catalyst regeneration. Surprisingly, persulfates activity restored to the initial level at ND-2000 outperforming other metal nanoparticles like zerovalent iron (Fe°) or manganese dioxide (MnO_2) nanoparticles [32] in removing 4-Chlorophenol. This effect could be explained by the high electrical conductivity of graphitized nanodiamonds as well as the removal of inactive graphitic layers of this ion-like surface by photo-oxidation processes.

It was indicated that the persulfate-based AOPs involve the various mechanisms: (I) nonradical oxidation pathways engaging generated singlet oxygen and (II) nonradical oxidation pathways driven by sulphate or hydroxyl radicals (see Figure 4B) [33]. Target organic pollutants react with oxidants ($SO_4 \bullet^-$ and $\bullet OH$) in the analogous steps including (1st) hydrogen abstraction, (2nd) electron transfer, and (3rd) addition varying just on the reaction kinetics. Thus, a direct comparison of oxidant role has to be studied for each pollutant comparing the potential role of $SO_4 \bullet^-$ versus $\bullet OH$. In the case of $\bullet OH$-driven oxidation, hydrogen is abstracted from carbons in the aliphatic chain attached to the carboxyl group followed by carbon-centred radicals formation. Next, they react with oxygen and by-products resulting from Russel- or Bennett-type reactions. Furthermore, $SO_4 \bullet^-$ radicals are responsible for electron abstraction from oxygen in the carboxyl group. Nevertheless, it was also claimed that singlet oxygenation is a more reliable pathway mechanism than the radical pathway theory [34]. It was revealed that $^1O_2$ is formed through the decay of peroxy-acids (*i.e.,* PMS).
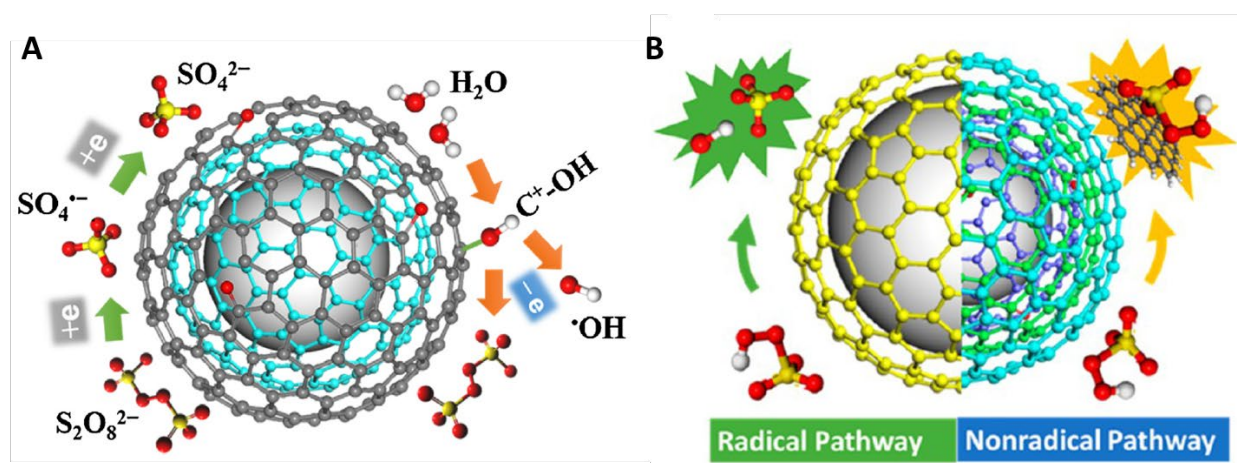
Figure 4. (A) Mechanism of a radical pathway of persulfate activation process occurred at annealed nanodiamond. Reproduced with permission from Ref. [31]. Copyright 2016, Elsevier. (B) Scheme of radical and non-radical pathways revealed at G-ND. Reproduced with permission from Ref. [30]. Copyright 2018, Elsevier.

The •OH radicals could be formed directly from asymmetrical PMS (see Eq. 1) while activation of symmetrical PDS is highly dependent on the $SO_4^{\bullet-}$ and H_2O (see Eq. 2) [35]. $SO_4^{\bullet-}$ radical is dominating at neutral pH. The AOP starts to be dominated by •OH radicals at pH > 9 in agreement with the reaction shown in Eq. 3.

$$HSO_5^- + e^- \rightarrow {}^{\bullet}OH + SO_4^{2-} \tag{1}$$

$$SO_4^{\bullet-} + H_2O \rightarrow H^+ + SO_4^{2-} + {}^{\bullet}OH \tag{2}$$

$$SO_4^{\bullet-} + OH^- \rightarrow SO_4^{2-} + {}^{\bullet}OH \tag{3}$$

Next, wastewaters usually reveal high salinity levels diverting selective remediation processes. In such a complex media, the sulphate radicals could react with Cl^- forming $Cl^{\bullet}$ which then could react with chloride ions forming chlorine radicals like $Cl_2^{\bullet-}$ [31], turning into a remarkably significant process at low pH. The studies focused on real wastewater installations are a challenging task, which should be extensively investigated. As stated above, the oxidation processes in the persulfate / ND system are complex and interdependent, thus its final mechanism is still debatable.

In addition, Duan *et al.* [14] reported that controlled thermal annealing with N-rich precursor (e.g., melamine) provides nitrogen doping enhancing both electrochemical performance along with peroxymonosulfate (PMS) activation. N-doped *sp²* graphitic shells reveal improved charge transfer thanks to tuned bandstructure tailored by variously positioned nitrogen atoms. The analogous effect was achieved by deeply oxidized nanodiamond in nitric acid (70%), which allowed for improved and volume doping of both diamond core and graphitic shell regions [31]. Nitrogen doping level was investigated by X-ray photoelectron spectroscopy conducted priorly and after treatment process revealing respectively 9.18 and 0.92 at% of oxygen and nitrogen in the diamond particles. The fitted N1s spectra revealed the formation of amino groups, pyridinic N, graphitic N, and nitric oxides on the surface (see Figure 5A). Next, the oxynitrides were removed during thermally induced pyrolysis. It should be also noticed that DND particles contain residual nitrogen content thanks to the nature of their synthesis.

Due to the above facts, the strong EPR signals were recorded attributed to the large amount of generated reactive radicals as displayed in Figure 5B. The increased levels of sulfate and hydroxyl radicals were achieved by nitrogen doping proving that PMS was activated more efficiently inducing faster total phenol degradation in just 60 minutes in comparison to previous works [30] conducted at undoped nanodiamonds. Figure 5C presents a decrease of reaction rate constants from 0.072 to 0.035 min^{-1} once tert-butanol or ethanol was additionally used during the oxidation process. Both compounds used to quench hydroxyl radicals with high reaction rates proving the dominant role of mentioned species in phenol oxidation. Doping of ND by nitrogen results in considerably modified charge distribution attributed inter alia to the larger electronegativity of N relating to C [31]. The positively charge C atoms enhance activation of O-O bonds, while N atoms play as

Lewis's basic sites improving electron transfer. Both effects accelerate the activation of PMS catalyzing pollutant removal.
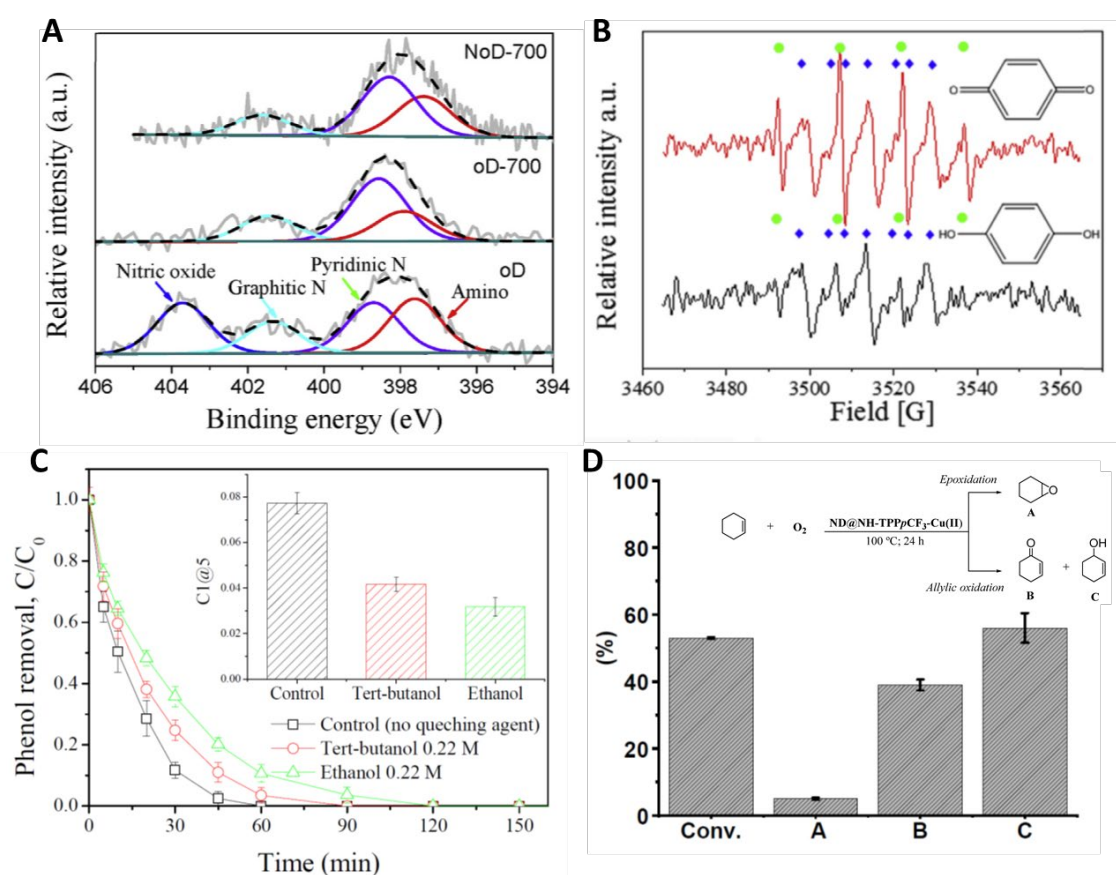
Figure 5. (A) N1s high-resolution spectra of annealed nanodiamonds; (B) EPR spectra of peroxymonosulfate catalysis, (C) Reactive species produced during phenol removal at N-AND/ peroxymonosulfate. Reproduced with permission from Ref. [31]. Copyright 2016, Elsevier. (D) The % efficiency of cyclohexene oxidation catalyzed by using copper(II)–porphyrin complexes grafted at nanodiamond (Inset: by-product selectivity). Reproduced with permission from Ref. [36]. Copyright 2020, MDPI (Basel, Switzerland).

The activation capacities of PMS/ND systems are considerably improved with increasing conductivity of graphitized nanodiamonds. Yun *et al.* [37] noticed the increase of currents at electrodes coated with the graphitized nanodiamonds occurred when exposed to the electrolyte containing PMS and 4-chlorophenol (4-CP) revealing oxidation reactions. The observed electron transfer induced by organics injection indicates that an electron donation to PMS (electron acceptor) is aided by nanodiamonds recognized as green charge-transport mediators. It was revealed that PDS-assisted oxidation results in the dichlorination and hydroxylation of 4-CP [31]. The longer oxidation processes result in the generation of quinone intermediates (hydroquinone and benzoquinone), which could be mineralized applying raised doses of PDS.

Besides broad use of persulfates, Sato *et al.* [38] applied nanodiamond–copper(II)–porphyrin (ND@NH-TPPpCF3-Cu(II)) complexes to treat cyclohexene applying oxygen. Covalent bonding of porphyrin complex to nanodiamond utilizing plan model *Allium cepa* allowed for the design of low-fitotoxic "green" carbocatalysts. Figure 5D exhibits 53% conversion of cyclohexene to the various by-products B—2-

9

cyclohexen-1-one or C—2-cyclohexen-1-ol attributed mostly to the allylic species. Lately, Brun *et al.* [39] irradiated hydrogenated (H-ND) and oxidized (O-ND) nanodiamonds by MeV photons achieving the rapid generation of hydroxyl radicals and solvated electrons in aqueous solution inducing radiolysis, which causes organics oxidation and other interfacial processes.

Table 1. Removal of organic compounds by oxidation using nanodiamonds and diamond-based nanostructures.

Process	ND type (catalyst / reactant)	Oxidants	Target pollutant	Conditions	Removal efficiency	Reference
AOP	G-ND / PMS or PDS	•OH and SO_4•−	bisphenol A, phenol, 4- chlorophenol, 2,4,6-trichlorophenol,	50 mL at RT, aqueous 0.1 mM target organic substrate, 0.5 mM PDS, and 0.05 g/L thermally treated ND, pH 3-11	100% in 1-3h depending on the conditions	[23]
AOP	G-ND / PMS	•OH and SO_4•−	real river water, phenol	50 ml suspensions containing carbon nanomaterial, target organic compound, pH 7 at RT	100% in 1h	[24]
AOP	N-doped G-ND / PMS	•OH and SO_4•−	phenol	250 mL batch reactor with phenol solution (20 ppm), catalyst (0.2 g/L) and PMS (6.5 mM), pH =7.00 at RT	100% in 45 mins	[31]
AOP	N-doped ND + PDDA+GO / PMS	•OH and SO_4•−	bisphenol A, carbamazepine,, 4-chlorophenol (4-CP), 4-nitrophenol , nitrobenzene phenol , 2,4,6-trichlorophenol	50 mL batch reactor, 0.1 g/L ND-based activator, 1mM PMS, and 0.1mM target substrate, aqueous suspensions buffered at pH 7.0 and RT	4-CP 100% in 50 mins	[37]
AOP	Annealed ND / PMS	•OH, SO_4•− and nonradical oxidation on carbon surface	phenol, methylene blue, catechol, sulfachloropyridazine	20 ppm phenol solution was prepared from a 1000 ppm phenol stock solution with a pH of 5.9 at RT	100% in 45 mins	[40]
AOP	Annealed ND / PMS	singlet oxygen	4-chlorophenol	100 mL beaker at 20 ± 2 °C, pH value of reaction system was not adjusted, 5 mg of catalyst in 50 mL of the 4-CP solution, PMS 0.25 × 10⁻³ M	100% in 30 mins	[29]
Catalytic ozonation	G-ND	hydroperoxyl and $^1O_2$	oxalic acid	aqueous pollutant (50 mg/L; 250 mL) together with the dispersed NDs (100 mg/L) in the glass reactor , pH 3 at RT	100% in 3h	[41]
EAOP	BDD at carbon fibers	•OH	phenol or tetracycline	10 mL of 50 mg L⁻¹ representative pollutant,	100% in 3h /	[42]
EAOP	B-doped ND	•OH	2-chlorophenol	EC compartment 100 mL of 100 mg/L 2-chlorophenol solution, 0.2 M Na₂SO₄, current density 20 mA/cm⁻² with pH 3.5 and 7 and at 25 °C	98% in 6 h	[43]
EAOP	BDD / PDS/PMS	•OH	carbamazepine (CBZ)	electrolysis divided by a cation exchange membrane into two	100% in 20 mins	[44]

chambers with 90 mL net
volume, NaClO$_4$
electrolyte with PDS 5
mM, current density =100
A m^{-2}

*Abbreviations: RT – room temperature, PDDA - poly(diallydimethylammonium chloride), EAOP – electrochemical AOP.

Furthermore, graphitized nanodiamond was also manifested as effective ozonation catalysts in water (annealed in Ar at 1100°C for 1 h) [41] allowing for O$_3$ transformation into hydroperoxyl radicals and ^{1}O$_2$ oxidants. Bernat-Quesada *et al.* [41] reported catalytic ozonation of oxalic acid applying G-ND. Generation of oxygen species was attributed to electron delocalization in π-conjugated carbonyl groups at G-ND surface donating electrons to O$_3$.

Moreover, green-oriented AOP was achieved combining PDS and PMS activation jointly with electrolysis at BDD. Song *et al.* [44] showed that electrochemically activated persulfates increase removal rates of carbamazepine (CBZ). The effect was attributed to much higher concentrations of hydroxyl radicals adsorbed at BDD surface generated by sp^2 impurities in the anodes. Surprisingly, the combined process results in the production of the limited intermediate enabling much lower toxicity at relatively low energy consumption. Kondo *et al.* [16] proposed novel electrode fabrication for electro-oxidation based on the boron-doped diamond powders (BDDP) composite electrodes mixed with polymers, which could be used as an ink-like coating. The standard electro-oxidation remediation process usually is conducted at polycrystalline boron-doped diamond (BDD) anodes [45,46]. Boron-doped nanodiamond powders were fabricated in the typical CVD growth procedure using natural diamond seeds. BDDP could be deposited on temperature-sensitive substrates (ie. Vylon [47] or Nafion [16]) utilizing screen-printing technique. Such an electrode reveals high efficiency in ozone and oxidative intermediates generation. The treatment of *Porphyromonas gingivalis* at BDDP-polymer electrode by advanced oxidation process allowed to suppress biofilm formation in the human tooth. Just 120 seconds of exposure in 1% NaCl causes almost 100% degradation of organic colonies versus blank control sample treated in PBS. Importantly, BDD anodes could generate high local concentrations of active •OH radical demonstrating 100,000 times higher efficiency than that of chlorine enabling rapid mineralization and disinfection [48].

Nanostructured BDD could be also achieved by growing diamond at porous titania, titania nanotubes, etched Si, nickel foam resulting in enhanced removal rates of organic pollutants thanks to the higher surface area, adsorption capacity and electron transfer [49]. Yang *et al.* [42] manifested recently that nanostructured carbon fibers overgrown by BDD could be applied for electrocatalytic degradation of organic pollutants (e.g. methyl orange, phenol, or tetracycline). This high specific area and efficient electrocatalyst is a promising and competitive approach to the presented above ND-based and persulfate-driven oxidation processes. Liu *et al.* [50] reported and superior activity for electro-reductive degradation of emerging pollutant 2,2`,4,4`-tetrabromodiphenyl ether (BDE-47). The process was conducted at vertically aligned nitrogen-doped nanodiamond (VA-NDD) grown at Si rod arrays (Si-RA). Designed electrodes showed a 95% factor of BDE-

11

47 (20 mg/L) reduction in just 120 minutes. Remarkably, VA-NDD/Si-RA reveals improved efficiency relating to standard BDD grown at the same Si array, graphitic, Pt, or Pd electrodes. Nitrogen-doped electrodes exhibited excellent hydrogen evolution with much more negative potentials in comparison to standard BDD, because N-doping induces sp^2 defect introducing catalytic sites. Moreover, NDD electrodes result in a larger specific surface area facilitated by their nanocrystalline nature. Nitrogen doping tuning band structure of diamond improving surface conductivity mediated by both sp^2 and sp^3 phases. These synergistic effects induced by approx. 2% of nitrogen doping delivering improved hydrogen evolution as revealed also previously by other groups [51]. Recently, Ajeel *et al.* [43] achieved diamond nanoparticles doping by boron utilizing thermally induced pyrolysis at boric acid atmosphere (up to 1100^oC). The doping process was conducted at pristine diamond (P-ND) and annealed diamond particles (A-ND). Particles were applied for degradation of 2-chlorophenol by electrochemical treatment. Analogously to the catalytic works, the A-ND revealed higher anodic oxidation activity and manifested a 98% removal rate of 2-chlorophenol after 6 h of treatment. Reduction of pH from 7 to 3.5 increases removal rates of *ca.* 25% since the hydroxyl radicals oxidation potential is enhanced and phenolic compounds decrease their dissociation energy at low-pH electrolytes. Noteworthy, phenolic intermediates could also passivate electrode surface in high pH.

3. Photocatalytic degradation of pollutants using nanodiamond induced oxidation

Unique photocatalytic degradation of NDs was recognized once they were merged with semiconducting materials as Cu_2O [52], TiO_2 [53], or C_3N_4 [15], thanks to the formation of relatively large area photoactive heterojunctions with enhanced light scattering performance. Such an approach provides increased charge generation and extended lifetime of carriers delivering photocatalytic activity for the hydrogen evolution towards pollutants treatment under visible light.

Henych *et al.* [53] reported that TiO_2/ND composites enhance reactive adsorption and solar light photodecomposition of dimethyl methyl phosphonate (DMMP) or highly toxic OP soman. They revealed that admixture of ND improves the adsorption capacity and thus a the adsorbed DMMP can be decomposed faster by photo-induced reactive species (see Figure 6A). Surprisingly, once ND coverage becomes excessively thick the effect is suppressed implying hindering of TiO_2 by tight physical contact of TiO_2/ND composites. ND admixture considerably modifies texture and porosity of composite resulting in the higher adsorption capacity acting simultaneously as an electron mediator for TiO_2 reducing electron-hole recombination.

Similar TiO_2/ND composites were studied by Sampaio *et al.* [54] reporting degradation of microcystin-LA (attn. widespread cyanotoxin) employing the photocatalytic approach utilizing both simulated sun and visible light sources. Figure 6B displays TiO_2/ND performance showing pseudo-first-order rate law by using solar light, while reference blank test with no catalyst revealed lack of productivity proving resistance of microcystin-LA to direct photolysis. The synergistic effect of TiO_2/ND composites results in almost 15 times improved degradation kinetics but just under simulated solar source exposure.
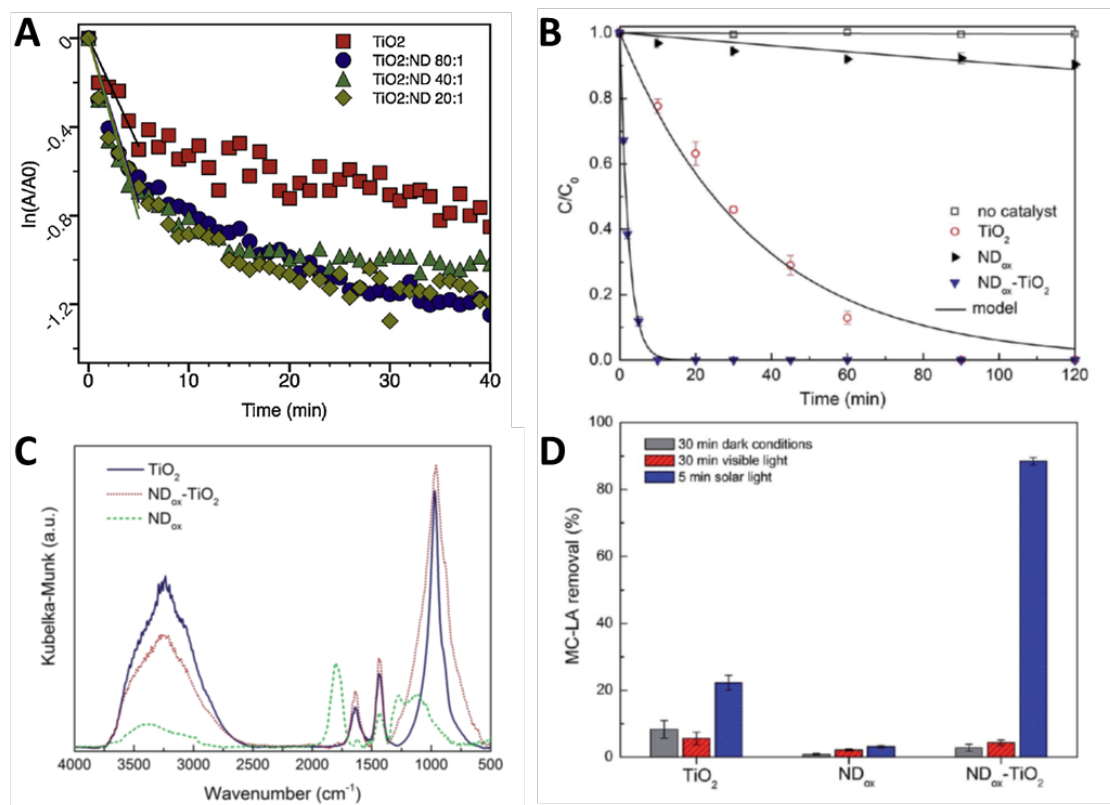
Figure 6. (A) Logarithmic decay of the C–H stretching representing the efficiency of photodegradation induced by TiO2/ND nanocomposites. Reproduced with permission from Ref. [53]. Copyright 2016, Elsevier. (B) Time evolution of microcystin-LA (attn. cyanotoxin) degradation employing TiO_2/ND nanocomposites, (C) Diffuse reflectance spectra of nanodiamond – TiO_2 complexes, (D) Cyanotoxin removal versus various light conditions. Reproduced with permission from Ref. [54]. Copyright 2015, Royal Society of Chemistry.

To investigate the photocatalytic effect of TiO_2/ND complexes with aqueous media, the diffuse reflectance infrared Fourier transform (DRIFT) technique was applied (see Figure 6C). The DRIFT spectra manifest wide bands in the 2500-3800 cm^{-1} range attributed to the stretching vibrations of surface-bonded water molecules and hydroxyl species, while the low-intensity band positioned at 1640 cm^{-1} was coupled with Ti–OH bonds.

It should be noted that much weaker photocatalytic performance, compared in Figure 6D, was achieved during irradiation by visible spectrum range (Vis). This phenomenon could be credited to the widening of bandgap by admixed NDs, therefore, weak light absorption in the Vis spectral range. The reference dark experiments showed up to 8% decrease of microcystin-LA in 30 minutes defining adsorption equilibrium between compounds.

Next, Su *et al.* [15] elaborated a unique heterojunction linking boron-doped nanodiamonds (BDND) with graphitic carbon nitride nanosheets (g-C$_3$N$_4$) utilizing the pyrolysis technique. Figure 7A displays recurring on-off photocurrent plots recorded under Vis range light manifesting almost doubled catalytic performance of BDND@g-C$_3$N$_4$ versus pristine g-C$_3$N$_4$.

Analogous results were revealed utilizing double-approach heterostructure consisting of Ag nanoparticles and undoped nanodiamonds coupled with g-C$_3$N$_4$ [55]. Nevertheless, such an approach is much more simplified

13

in fabrication and exhibits almost 5 times improved H2 evolution during water splitting experiment and more than 2 times increased organic pollutants degradation using visible-light source (compared in Figure 7CD).

The improvement by Ag photocurrent density (Figure 7B) was attributed mostly to the induced simultaneously surface plasmon resonance effect increasing separation of photogenerated electron-hole pairs and tuning light absorbance.
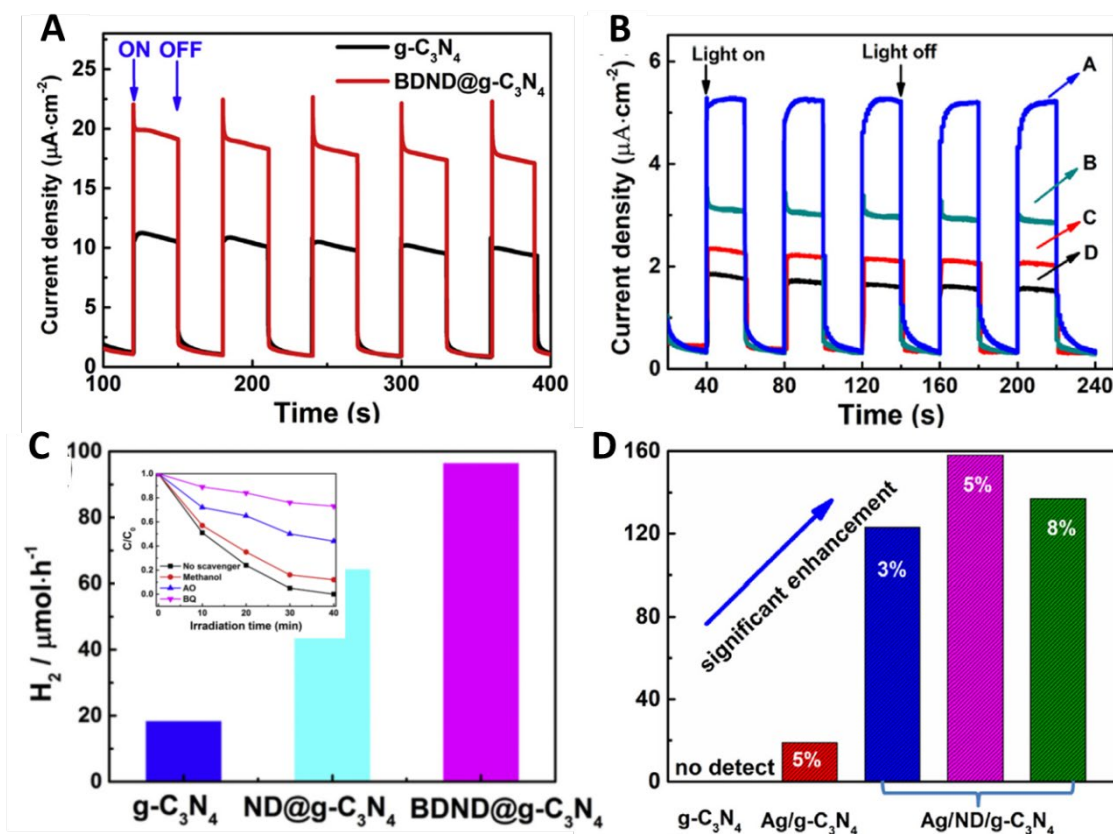
Figure 7. (A) Light-induced current boron-doped nanodiamonds grown at g-C_3N_4 nanosheets, (C) Hydrogen evolution at various g-C_3N_4 / diamond heterostructures under visible-light irradiation (Inset: photocatalytic degradation of rhodamine B in aqueous solution), Reproduced with permission from Ref. [15]. Copyright 2019, Elsevier. (B) Tunning of photocurrents by g-C_3N_4 / diamond heterostructures supplied by Ag (Attn. A: Ag/ND/g-C_3N_4, B: ND/g-C_3N_4, C: Ag/g-C_3N_4, D:g-C_3N_4), (D) Photocatalytic H2 evolution versus different loading of Ag. Reproduced with permission from Ref. [55]. Copyright 2020, Elsevier

The trend in Figure 7C clearly shows that the addition of NDs or BDND efficiently boosts the H2 evolution rates in comparison with pristine g-C_3N_4. ND mostly contributes to the effect by increased light scattering and electron-hole pairs separation, while BDND enhances absorbance in the Vis range. Additionally, inset in Figure 7C displays variation of photocatalytic degradation of rhodamine B (RhB) performed in the aqueous solution of methanol (1 mM), ammonium oxalate (AO) (1 mM), and p-benzoquinone (BQ) (1 mM) playing the role of quenchers for hydroxyl radicals (•OH), holes, and superoxide radicals (•O_2^-), respectively. The concentration of RhB was investigated by measurements of the absorbance spectra at 554 nm.

First, methanol just slightly inhibits the RhB degradation revealing that •OH radicals are not the crucial factor of photocatalytic activity. Notably, the photodegradation rate of RhB was considerably suppressed by radical

14

quenchers (AO or BQ) implying that photo-generated holes and $\bullet O_2^-$ are the main species responsible here for photocatalytic degradation of organic pollutants. Su *et al.* [55] optimized also surficial Ag concentration revealing that a large concentration of silver suppresses photocatalytic H_2 evolution of that complex (see Figure 7D), while bare g-C_3N_4 or ND/g-C_3N_4 does not exhibit observable photocatalytic effect at all. The 8% of Ag nanoparticles probable induces the barrier for light or the forms centers for potential recombination of electron-hole pairs.

Wang *et al.* [56] proposed to modify ND surfaces by pyridine groups bonding them with Ag nanoparticles and improving dispersity of such plasmonic complexes in various solvents. Such a heterostructure allowed for direct photodegradation of methyl blue (MB) with visible light, observed as medium decolorization. The energy transfer from Ag nanoparticles facilitated by localized surface plasmon resonance was revealed as a major mechanism pushing a photocatalytic effect.

A comparable modification scheme was proposed by Liu *et al.* [57] decorating NDs by ZnO targeted for toluene removal utilizing UV-365 light source. The high-resolution TEM image displayed in Figure 8A revealed direct interaction of homogeneous ZnO/ND complexes and uniform coverage by ND crystals. Figure 8B summarizes the time evolution kinetics of gaseous toluene removal using the photocatalytic approach. Reference blank test at bare ZnO or without illumination does not exhibit a reduction in toluene concentration. Obviously, ND admixture induces photooxidation process resulting in almost total removal of toluene in 120 minutes with high reproducibility studied during five reaction cycles. Toluene degradation corresponds closely with CO_2 generation introduced by ND-induced optical absorption and transient photocurrents. NDs promoted here also charge transfer revealed by impeded photoluminescence and electrochemical impedance.

Intriguingly, Li *et al.* [58] designed PVDF-based membranes loaded with TiO_2 and carboxylated NDs (CNDs) showing enhanced photocatalytic effect thanks to their porosity and antifouling mainly due to rich hydrophilic groups. Inset in Figure 8C displays a photo of carboxylated nanodiamond loaded TiO_2/PVDF membrane after 90 minutes of methylene orange dye (MO) photodegradation under simulated solar irradiation. The COOH-ND/TiO_2/PVDF membrane allows achieving over 80% of MO degradation being slightly more efficient than pristine TiO_2/PVDF (see Figure 8C).

Time-resolved evolution of MO decomposition kinetics, presented in Figure 8D, showed that both COOH-ND/TiO_2/PVDF and TiO_2/PVDF follow the same linear MO reduction trend, while bare PVDF or COOH-ND/PVDF exhibits catalytic process saturation after approx. 20 minutes. Studies suggest that the photocatalytic effect is mostly driven by TiO_2, while COOH-ND improves it by complexing with TiO_2 limiting adsorption capacity and thus fouling of the membrane.

15
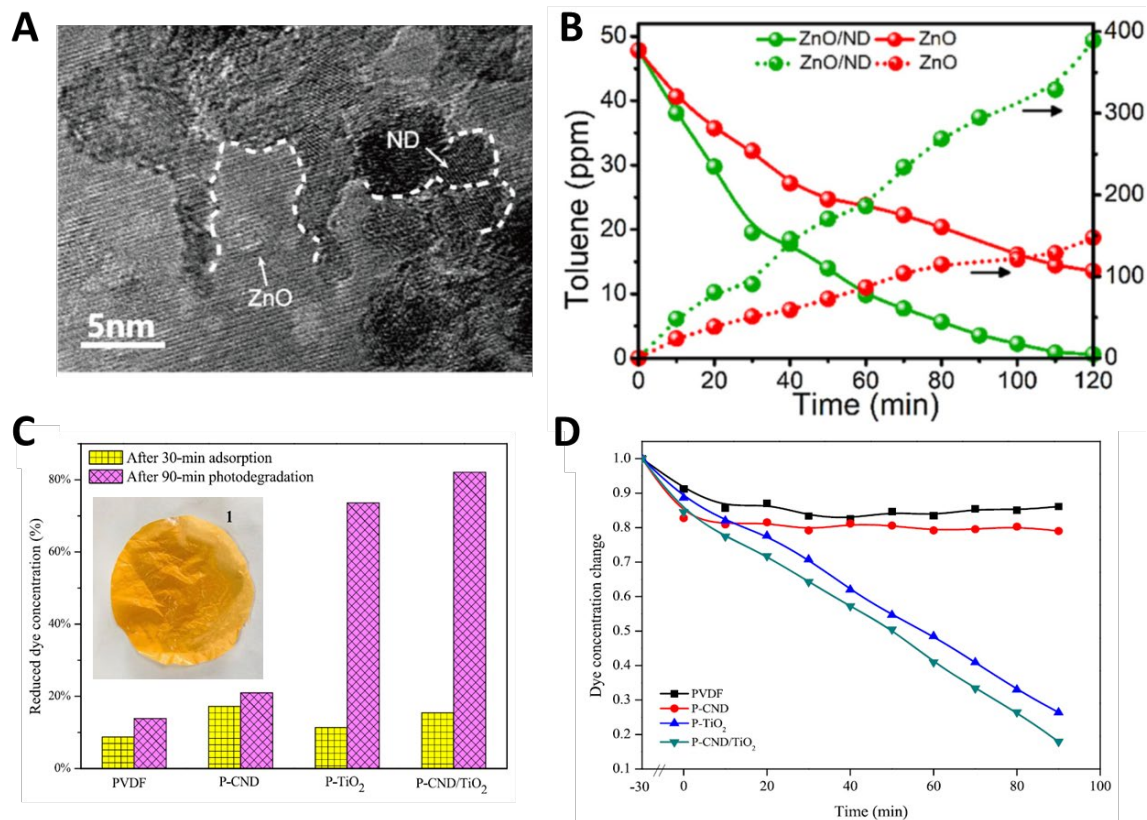
Figure 8. (A) The dark-field microscopic image of ZnO-nanodiamond composite, (B) Toluene and the CO_2 yield at ZnO-nanodiamond catalyst complexes. Reproduced with permission from Ref. [57]. Copyright 2019, Elsevier. (C) Variation of dye removal after adsorption in the dark and photodegraded under solar irradiation in the function of an applied membrane (Inset: Photo of carboxylate nanodiamond loaded TiO_2/PVDF membrane. (D) Time-resolver dye removal at various nanodiamond-loaded membranes. Reproduced with permission from Ref. [58]. Copyright 2015, American Chemical Society.

The addition of nanodiamond tailors performance of above-mentioned complexes but its exact role and mechanism standing behind observed photocatalytic effect enhancement is still not evident mostly due to electronic heterogeneities tuning band structure and ambiguous surface chemistry. Several refereed works report on the mechanisms showing the roles and pathways of major species as well charge transfers. Figure 9 summarizes essential processes of photocatalytic degradation induced by ND complexes. First, the ZnO/ND complexes allow for generations of light-stimulated electron-hole pairs used in process of toluene degradation [57]. ND performs as electron source transferred to ZnO forming $\bullet O_2^-$ radicals from oxygen, whereas ZnO produces holes transported to ND reacting with ZnO and contributing directly to toluene oxidation. The standard redox potential of $\bullet OH/H_2O$ is placed here above the valance band of photocatalyst, thus, $\bullet OH$ radicals are not produced. In general, toluene could undergo the following mineralization pathway (see Figure 9A): (I) rapid reaction with $\bullet O_2^-$ producing benzaldehyde and benzoic acid; (II) oxidation of benzoic acid to oxalic acid followed by decomposition to both CO_2 and water by aromatic ring breaking; (III) benzaldehyde and benzoic acid could also form benzene and hydroxylated intermediates being problematic in the farther mineralization.

16
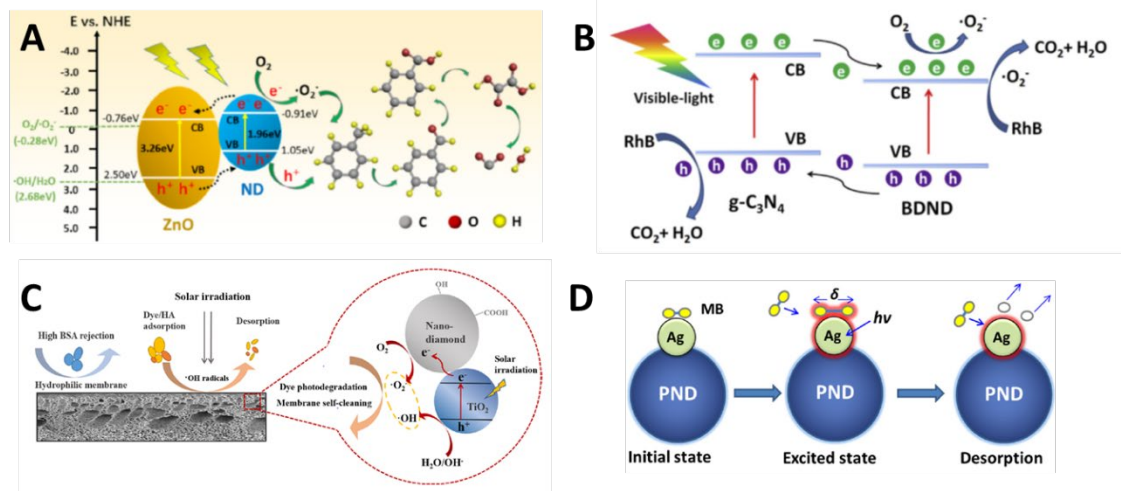
Figure 9. (A) Mechanism for photocatalytic degradation of toluene using nanodiamond - ZnO complexes. Reproduced with permission from Ref. [57]. Copyright 2019, Elsevier. (B) Enhanced photocatalytic degradation of rhodamine B at boron-doped nanodiamond at g-C_3N_4 nanosheets. Reproduced with permission from Ref. [15]. Copyright 2019, Elsevier. (C) The self-cleaning effect at complex photocatalytic membrane PVDF−carboxylated nanodiamond/TiO_2, Reproduced with permission from Ref. [58]. Copyright 2015, American Chemical Society, (D) Process of plasmon-induced photodegradation of methylene blue using silver deposited at pyridine modified nanodiamonds. Reproduced with permission from Ref. [56]. Copyright 2015, Elsevier.

Figure 9B illustrates an energetic diagram of BDND/g-C_3N_4 heterojunction, where valence (VB) band of boron-doped diamond was estimated as 1.95 eV, while conduction band (CB) was placed at 0.48 eV. BDND serves as an electron acceptor due to lower CB although both species generate electrons. Next, the large amount of holes supplied by BDND leads to the transfer of photogenerated electron-hole pairs towards the interface decreasing the recombination effect [15]. Additionally, BDND/g-C_3N_4 exhibits considerable narrowing of bandgap relating to bare g-C_3N_4 enhancing photoelectron excitation. They induce directly dominant reactive species (holes, hydroxyl •OH and superoxide anion •O_2^- radicals) providing mineralization of RhB to CO_2 and water. The carriers transport and pairing are analogous with the phenomenon described for ZnO/ND complexes.

A similar synergetic effect was reported for PVDF membranes loaded by carboxylated NDs (CNDs) and TiO_2. Figure 9C shows membrane cross-section along with photo-mechanism elaboration based on the production of electron-hole pairs under sunlight irradiation. As already mentioned, holes are responsible for •OH radicals production from H_2O. Mostly, the photogenerated electrons transferred to CNDs induce the effective hole/electron separation delivering overproduction of oxidation species and, thus, dye degradation [58].

At least, ND could be loaded by Ag nanoparticles inducing direct plasmonic photocatalytic performance as sketched in Figure 9D [56]. Visible light was applied to excite Ag nanoparticles forming localized surface plasmon resonance with high free electrons mobility, which are accounted for forming methylene blue (MB) ions with long covalent bonds to silver. During the electron relaxation process the cleavage of those bonds (δ) leads to the dye chromophores mineralization into CO_2 and H_2O. Nanodiamond plays here as an energy harvester and attenuator of MB-Ag complexes formation.

17

4. Functionalized nanodiamonds designed for adsorptive removal of organic contaminants

Finally, nanodiamond particles could be utilized as active medium facilitating adsorption of organic pollutants. Beltz *et al.* [59] conducted extensive studies of adsorption and release of tiopronin at functionalized nanodiamond surface for drug delivery. Nevertheless, the multifunction and flexible chemistry of nanodiamond surfaces serve also as efficient adsorption facilitators for pollutants removal.

Çiğil *et al.* [60] functionalized detonation nanodiamond surfaces by hybrid polyethyleneimines driving Pb(II) uptake process (see Figure 10A). The photopolymerized urethane acrylate, trimethylolpropane triacrylate (PEI), and glycidyl methacrylate monomers (GMA) provided binding of metal ions due to diversely oriented amine groups. Apparently, the adsorption process exhibits saturation point (ca. 17 mg g^{-1}) in 7 hours due to the limited number of groups for ion uptake. Such a high efficiency was achieved thanks to the opened epoxy groups in GMA induced by PEI coexistence.
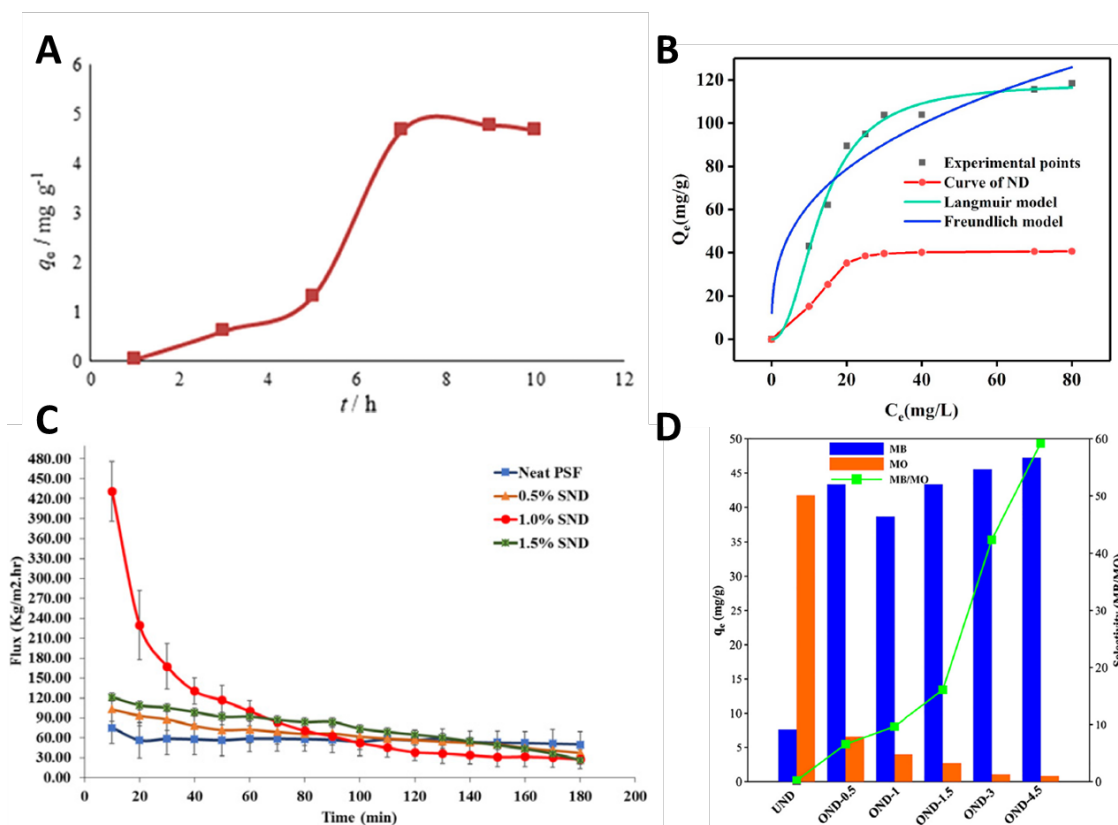
Figure 10. (A) Pb (II) uptake capacity of nanodiamonds modified by polyethyleneimine. Reproduced with permission from Ref. [60]. Copyright 2019, John Wiley & Sons, Inc. (B) Cu (II) adsorption at ionic copolymer modified nanodiamonds supplied by Langmuir and Freundlich models. Reproduced with permission from Ref. [61]. Copyright 2020, Elsevier. (C) Humic acid removal filtration at silanized nanodiamond in the polysulfone (PSf) membrane. Reproduced with permission from Ref. [62]. Copyright 2020, Elsevier. (D) Adsorption selectivity of methylene blue over methyl orange for different nanodiamonds. Reproduced with permission from Ref. [63]. Copyright 2018, Elsevier.

Other ions like Cu(II) could be also chelated at hydroxylated nanodiamonds (ND-OH) synthesized by Diels-Alder reaction using furfuryl alcohol [61]. This reaction results in electronegative acrylic acid (AA) and 2-

18

methacryloyloxy ethyl phosphorylcholine (MPC) groups formation at nanodiamond surface ND-poly(AA-co-MPC) allowing for copper ions adsorptive removal by the large concentration of hydroxyl groups. Figure 10B compares Cu(II) experimental adsorption at modified nanodiamonds and simulated values supplied by both Langmuir and Freundlich models. Simulations allowed to reveal that Langmuir fits better to experiments than Freundlich isotherm model suggesting that chemical adsorption is dominant in the system. The maximum adsorption of pristine ND results in removal of 41.25 mg g^{-1}, while ND-poly(AA-co-MPC) significantly decreases the concentration of copper ions showing chelation of 118.7 mg g^{-1} depending slightly on the process temperature.

Notably, the silanized NDs incorporated in the polysulfone (PSf) membrane show high efficiency in humic acid (HA) adsorptive removal [62]. Figure 10C illustrates the kinetics of HA uptake induced by the antifouling performance of neat/pristine and vinyltrimethoxysilane-ND/PSf membranes. Up to 60 minutes of filtrations ND loading plays a considerable role in the adsorption process implying that process was considerably saturated after 1 hour of HA treatment. It was stated that HA filtration is mostly driven by hydrophilic nanodiamond surface modified by silanes, which tailors membrane wettability and thus fouling of the surface.

Popular surficial groups for biosensing as aryl diazonium salts gained recently widespread interest in adsorptive removal thanks to highly active sulfonic groups. Molavi *et al.* [63] reported that charged sulfonic surficial groups grafted to nanodiamond (ND-SO$_3$H) improves adsorption kinetics of methylene blue (MB) and orange (MO). Their studies revealed that just 3 minutes of MB exposure allows for instant absorption saturated after 15 minutes. ND-SO$_3$H allows for maximal MB uptake of 385.27 mg g^{-1} overwhelming considerably capacity of pristine NDs. The spontaneous adsorption is driven by an exothermic process tailored by reduced entropy of the complex. Moreover, the nanodiamond was thermally oxidized to tune the adsorption versus anionic and cationic dyes (*i.e.*, OND-1.5 means oxidized NDs for 1.5 h.).

Results shown in Figure 10D manifest that thermal oxidation of ND at 425°C promotes negatively charged cationic dyes over anionic favoured by UND (untreated). This effect is attributed to the formation of hydrogen bonds between the sulfonate groups of MO. Oxidized nanodiamonds (ONDs) revealed elevated adsorption capacity for MB mediated by the enhanced negative charge of annealed surface facilitating high electrostatic interactions.

Overall, the crucial role in the above-described processes plays pH of medium tuning removal performance, time-resolved kinetics, and reproducibility. Li *et al.* [64] designed covalently bonded Fe$_3$O$_4$/ND complexes fabricated using a polyglycerol mediator. Such a system was modified by immobilized HRP (horseradish peroxidase) to remove phenol from the aqueous solvent. The removal rates of phenol achieved 75 mg L^{-1}, but it was significantly pH-dependent mostly due to different activities of enzymes (see Figure 11A). The optimized 70-7.5 pH displaying high-level removal rates is contributed by the covalent bond between enzyme and ND stability [65], while free unbonded enzymes suffer from adsorption or decomposition.

Furthermore, the adsorption capacity of the above-mentioned sulfonate modified ND also depends on specific pH showing the variation of 70-75% efficiency-driven mostly by tuned electrostatics (see Figure 11B) [17]. The adsorption process could be here limited by that intra-particle diffusion phenomenon or π–π interactions regarding enhanced adsorption NDs-SO₃H. Nevertheless, this system shows much weaker variations versus pH than Fe_3O_4/ND complexes.
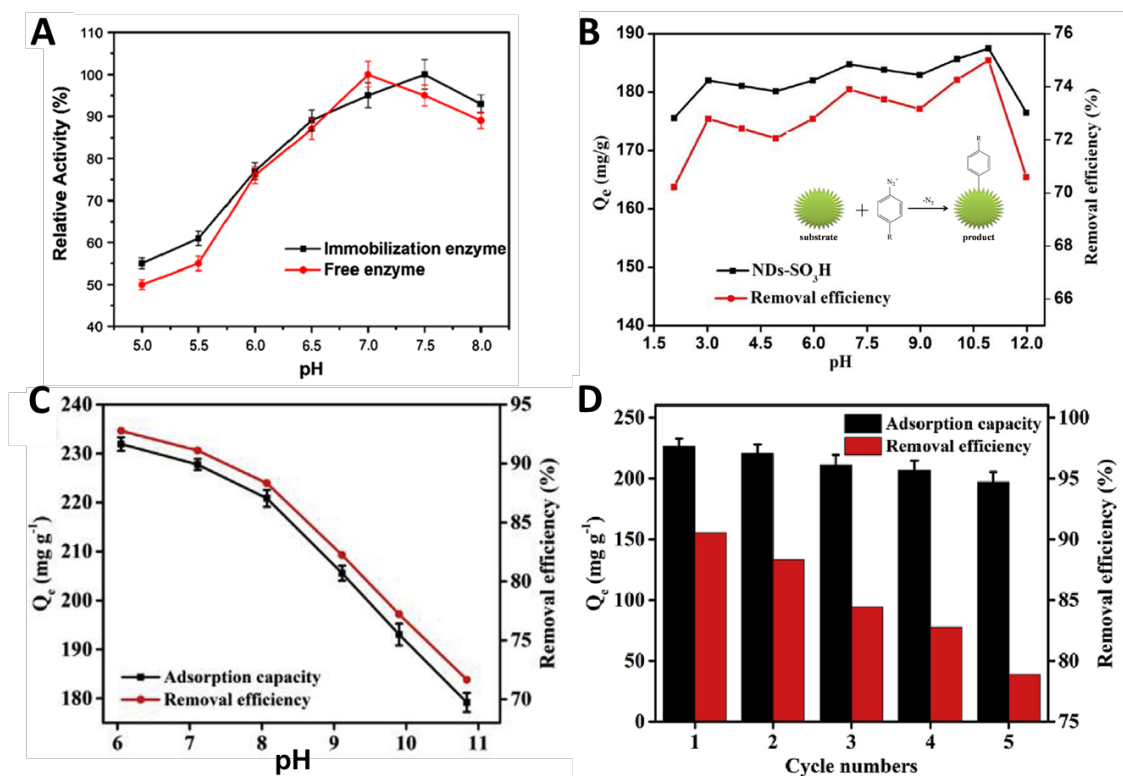
Figure 11. (A) pH influence on the immobilized enzymes and free enzymes at polyglycerol-functionalized magnetic Fe_3O_4/nanodiamond composites. Reproduced with permission from Ref. [64]. Copyright 2020, Springer Nature Switzerland AG. (B) Adsorption of methylene blue at sulfonated nanodiamond in the function of pH. Reproduced with permission from Ref. [17]. Copyright 2020, Elsevier. (C) pH dependence of Congo red removal at ionic liquid functionalized nanodiamonds, (D) Recyclability of ionic liquid functionalized nanodiamonds for the Congo red adsorption. Reproduced with permission from Ref. [66]. Copyright 2019, Elsevier.

Yang *et al.* [17] investigated the pH dependency of Congo red removal efficiency using ionic liquid modified nanodiamonds as shown in Figure 11C. The use of ternary ND@IL composites introduced amine groups at ND surface tailoring adsorptive removal of azo dyes. The observed Congo red adsorption capacities of pristine ND were 61.1 mg g⁻¹, while ND@IL reached 226.4 mg g⁻¹. Results of Congo red treatment reveal that pH sternly affecting adsorption tailoring surface charges. ND@IL was positively charged at pH < 7 attracting negatively charged dye molecules due to electrostatic interactions. For solutions pH > 7, the deionization of quaternary ammonium starts to play a crucial role in decreasing concentrations of positively charged regions suppressing Congo red adsorption. Next, the hydrophobic interaction between the alkyl chains and the dye molecule was also recognized as an important factor affecting adsorption processes.

In the next work of Yang *et al.* [66], the recyclability of ionic liquid functionalized nanodiamonds for the Congo red adsorption was investigated. Figure 11D presents five sequential cycles of Congo red adsorption revealing that ND@IL delivers reproducible adsorption capacity and removal efficiency. The slight reduction of dye removal efficiency of *ca.* 11% was observed ascribed to the defects-induced deteriorated hydrophobic interaction between adsorbent and dye molecule. Although, ND@IL was recognized as a highly efficient adsorbent competitive to the performance of NDs-SO$_3$H compounds [67].

Summary and Perspective

Summarizing, the presented review delivers a wide outline of the recent advancement and state-of-art status on the application of various nanodiamonds in the processes for the removal of emerging organic pollutants. Nanodiamonds are an interesting alternative to other nanocarbon catalysts due to their wide availability, relatively low costs, and, above all, a specific energy structure as well as a flexible surface susceptible to various functionalization strategies and modifications.

Conducting a thorough techno-economic analysis is practically impossible or very difficult due to the multi-parametric nature of the systems implementing AOPs. Additionally, the analysis must take into account the local specifics where the infrastructure will be implemented, the complexity of oxidized wastes, energy and maintenance costs. These types of installations are also particularly rare and usually have a pilot character where costs have not been optimized or effectively minimized. In addition, commercial installations are usually subjected to business secrecy and it is potentially not possible to know or publish the actual operating costs of a particular installation. Nevertheless, it should be stated, that the main cost of persulfate-driven PS-AOP is related to the reagents (*i.e.*, ND, persulfates) corresponding to more than 85% of the total treatment procedure [68]. The comparison of the cost/effectiveness ratio of the H$_2$O$_2$/UV-C, PMS, or PS/UV-C oxidation showed that processes involving H$_2$O$_2$ are still more economical [69]. Thus, the persulfates activation has to be improved to achieve an economically effective technology readiness level, which could be also possible by reagent cost reduction produced on the large scale. On the other side, the oxidation processes applying PS reveal higher operating costs in comparison to the conventional biological installations [70]. The electrochemical oxidation using boron diamond electrodes was recently considered highly competitive thanks to high O$_2$-evolution overpotential [71,72]. The electrochemical reactors are still lacking standardized reactor shape and electrode configuration required for industrial usage [73], thus extensive modelling and applied studies should be conducted to identify the optimal setup parameters. BDD-based AOPs system allowed for inactivation E. coli present in the secondary effluent of pH 7.6 with energy consumption of 2.24 kWh m^{-3} and energy costs 0.17 € m^{-3} [74]. Next, it was shown [75] that the minimal energy consumption reaches 2 kWh kg^{-1} of sodium peroxodicarbonate applying a current density of 720 mA cm^{-2}. Nevertheless, the high cost of BDD anodes fabrication ($26.5 × 10^3 m^{-2} [76]) and growing cost of energy facilitate the competitive role of other techniques as reviewed above ND-catalysed PS-based AOPs technology. The ND-oriented approach

enables relatively simplified scaling of the reactor for the utilization of organic compounds by increasing the volume. ND material is fairly available on the market (~couple of USD per carat) and could be reused in the remediation process once collected at the output membranes. Nevertheless, AOP processes are still demanding extended applied studies of oxidation pathways in complex media (*i.e.,* full wastewater, real river water, or sewage) to reveal their safety and meet the legal and environmental requirements.

Nanodiamonds offer also an efficient, durable, and stable platform inducing the course of many photocatalysis and oxidation processes with high reproducibility. The rate and density of their surface modification depend on the structure, defects, and impurities of ND particles. These parameters strictly depend on the type of synthesis used, the purity of its conduct, or further processing and cleaning processes after synthesis. Most of the works cited in the review concern generally particles derived from detonation synthesis because they are available on a larger scale, have lower sizes (typical few nm), and contain relatively higher initial concentrations of sp^2 phases. DND particles along with their thermally and chemically functionalized derivatives started to play an essential role as a PGM-free green catalyst. The unique synergy of sp^2 and sp^3 hybridized robust carbon matrix allowing to operate in extreme conditions powering catalytic reaction performance. Reviewed works manifested pollutants kinetics removal rates along with partial information on pathways and by-products showing their toxic and environmental impact.

On the other hand, they are prone to precipitation and agglomeration directly dependent on termination and further surface modification of nanocrystals. DNDs form various-size clusters following the stability of their surface termination, so an individual analysis and description of the mechanisms of the processes running on specific nanometric grains (2-10 nm) is practically impossible. Therefore, in most of the works presented in the review, the mechanism is described as the integral effect observed in the total weight/volume of DND powder. Practically these findings have not been linked directly to any specific surface processes at the monoatomic level. These issues in terms of diagnostics, optimization, and increasing the effect of pollutants removal are still not revealed and challenging. Theoretical modeling could be applied as a useful tool revealing pathways and mechanisms of reactions towards its engineering and optimization. However, the system is too large for DFT simulations, while molecular dynamics do not support simulations of electron distribution, which is responsible particularly for catalytic performance due to the delocalized π-electrons. The interpretations of B or N doping role in the bandgap engineering promoting charge transfer for carbocatalysis are still incomplete. Next, the effect of oxidants on the degradation pathways of target contaminants still needs additional studies, since the electrolyte type manifest substantial impact on the removal rates while much stable and potentially harmful oxidant chemicals are generated (*i.e.*, chlorates, or peroxydisulfate) [77]. Additionally, in the case of DND, it is difficult to discuss the influence of a particular crystallographic plane on the course of the modification processes and then the oxidation processes of various pollutants. This is an area for further interesting research and discoveries. An interesting alternative diamond product, still unexplored, is HPHT originated nanodiamond, the purity of which is much higher, having a much better

22

defined and organized surface, which would allow for the improvement of selectivity and engineering of modification processes and further reactions leading to applications, such as oxidation of a specific organic compound. The HPHT method is becoming more and more popular since its products are residuals in production for the jewellery market. Advanced sorting methods allow for HPHT to obtain specific groups of sizes along with defined facets, which will result in specific bandstructure and thus the pathways and mechanism of subsurface reactions. This is another perspective research field that opens broad opportunities and, at the same time, applications with improved repeatability. The presented broad spectrum of catalytic applications of NDs confirms that this type of material and its composites constitute a perspective design that could be effectively further developed, also combined with polymers, metals, or oxides, creating a new class of diamond composites that are green- and bio-friendly.

Nevertheless, the future perspective studies of wider application of persulfate-AOPs should take into consideration the field-tested operating practices allowing for mitigation of toxic by-products or side reactions in the real wastewater treatment. The large-scale sustainable and low-cost nanodiamonds are established but the industrial process has to be developed for the stabilization of its thermal treatment and impurities control. The reusability of nanodiamond or other carbocatalysts should be pushed forward since most of them should not be barely applied for water treatment due to their potential, still unknown environmental risks. It was already revealed that NDs cause severe toxicity to aquatic organisms as producers (e.g., cyanobacteria and microalgae), consumers (zebrafish or daphnia), or decomposers (e.g., bacteria and other microorganisms) [78]. Even if the NDs performance intimately depends on the specific aquatic system, the ND-based composite, membranes with rigid grafting of particles, and affordable cost should be considered as effective remediation platforms. Extended studies on assessing the risks and impact of such platforms are critical for society and ecosystems (*i.e.*, cellular toxicity or environmentally friendly sustainability). The coupling of AOPs with other water purification technologies such as membrane separation, adsorption, biomineralization, or capacitive deionization in the complex saline/industrial organic wastewater system should be challenged since such a synergistic approach could improve considerably treatment efficiency considering both economic and environmental impact factors.

Declaration of Competing Interest

The authors declare that they have no known competing financial interests or personal relationships that could have appeared to influence the work reported in this paper.

References

[1] N. Nunn, M. Torelli, G. McGuire, O. Shenderova, Nanodiamond: A high impact nanomaterial, Current Opinion in Solid State and Materials Science. 21 (2017) 1–9. https://doi.org/10.1016/j.cossms.2016.06.008.

[2] S. Stehlik, M. Mermoux, B. Schummer, O. Vanek, K. Kolarova, P. Stenclova, A. Vlk, M. Ledinsky, R. Pfeifer, O. Romanyuk, I. Gordeev, F. Roussel-Dherbey, Z. Nemeckova, J. Henych, P. Bezdicka, A. Kromka, B. Rezek, Size Effects on Surface Chemistry and Raman Spectra of Sub-5 nm Oxidized High-Pressure High-Temperature and Detonation Nanodiamonds, The Journal of Physical Chemistry C. (2021). https://doi.org/10.1021/acs.jpcc.0c09190.

[3] B.S. Miller, L. Bezinge, H.D. Gliddon, D. Huang, G. Dold, E.R. Gray, J. Heaney, P.J. Dobson, E. Nastouli, J.J.L. Morton, R.A. McKendry, Spin-enhanced nanodiamond biosensing for ultrasensitive diagnostics, Nature. 587 (2020) 588–593. https://doi.org/10.1038/s41586-020-2917-1.

[4] Y. Zhou, K. Zhao, J. Zhang, Y. Zhu, Y. Ma, H. Zhang, D. Song, X. Shi, L. Zhang, Y. Ding, Synergistic effects of nanodiamond modified separators toward highly stable and safe lithium metal batteries, J. Mater. Chem. A. (2021). https://doi.org/10.1039/D1TA03533A.

[5] A. Afandi, A. Howkins, I.W. Boyd, R.B. Jackman, Nanodiamonds for device applications: An investigation of the properties of boron-doped detonation nanodiamonds, Sci Rep. 8 (2018) 3270. https://doi.org/10.1038/s41598-018-21670-w.

[6] X. Duan, W. Tian, H. Zhang, H. Sun, Z. Ao, Z. Shao, S. Wang, sp2/sp3 Framework from Diamond Nanocrystals: A Key Bridge of Carbonaceous Structure to Carbocatalysis, ACS Catal. 9 (2019) 7494–7519. https://doi.org/10.1021/acscatal.9b01565.

[7] J.C. Arnault, H.A. Girard, Hydrogenated nanodiamonds: Synthesis and surface properties, Current Opinion in Solid State and Materials Science. 21 (2017) 10–16. https://doi.org/10.1016/j.cossms.2016.06.007.

[8] M. Ivanov, O. Shenderova, Nanodiamond-based nanolubricants for motor oils, Current Opinion in Solid State and Materials Science. 21 (2017) 17–24. https://doi.org/10.1016/j.cossms.2016.07.003.

[9] J.-P. Boudou, P.A. Curmi, F. Jelezko, J. Wrachtrup, P. Aubert, M. Sennour, G. Balasubramanian, R. Reuter, A. Thorel, E. Gaffet, High yield fabrication of fluorescent nanodiamonds, Nanotechnology. 20 (2009) 235602. https://doi.org/10.1088/0957-4484/20/23/235602.

[10] O.A. Shenderova, G. McGuire, 3 - Types of Nanocrystalline Diamond, in: O.A. Shenderova, D.M. Gruen (Eds.), Ultrananocrystalline Diamond, William Andrew Publishing, Norwich, NY, 2006: pp. 79–114. https://doi.org/10.1016/B978-081551524-1.50005-6.

[11] V.N. Mochalin, O. Shenderova, D. Ho, Y. Gogotsi, The properties and applications of nanodiamonds, Nature Nanotech. 7 (2012) 11–23. https://doi.org/10.1038/nnano.2011.209.

[12] M.H. Alkhatani, F. Alghannam, L. Jiang, A. Almethen, A.A. Rampersaud, R. Brick, C.L. Gomes, M.O. Scully, P.R. Hemmer, Fluorescent nanodiamonds: past, present, and future, Nanophotonics. 7 (2018) 1423–1453. https://doi.org/10.1515/nanoph-2018-0025.

[13] S. Navalón, A. Dhakshinamoorthy, M. Álvaro, H. García, Diamond Nanoparticles in Heterogeneous Catalysis, Chem. Mater. 32 (2020) 4116–4143. https://doi.org/10.1021/acs.chemmater.0c00204.

[14] X. Duan, C. Su, L. Zhou, H. Sun, A. Suvorova, T. Odedairo, Z. Zhu, Z. Shao, S. Wang, Surface controlled generation of reactive radicals from persulfate by carbocatalysis on nanodiamonds, Applied Catalysis B: Environmental. 194 (2016) 7–15. https://doi.org/10.1016/j.apcatb.2016.04.043.

[15] L.-X. Su, Z.-Y. Liu, Y.-L. Ye, C.-L. Shen, Q. Lou, C.-X. Shan, Heterostructured boron doped nanodiamonds@g-C3N4 nanocomposites with enhanced photocatalytic capability under visible light irradiation, International Journal of Hydrogen Energy. 44 (2019) 19805–19815. https://doi.org/10.1016/j.ijhydene.2019.05.135.

[16] T. Ochiai, S. Tago, M. Hayashi, K. Hirota, T. Kondo, K. Satomura, A. Fujishima, Boron-doped diamond powder (BDDP)-based polymer composites for dental treatment using flexible pinpoint electrolysis unit, Electrochemistry Communications. 68 (2016) 49–53. https://doi.org/10.1016/j.elecom.2016.04.011.

[17] Y. Lei, Q. Huang, D. Gan, H. Huang, J. Chen, F. Deng, M. Liu, X. Li, X. Zhang, Y. Wei, A novel one-step method for preparation of sulfonate functionalized nanodiamonds and their utilization for ultrafast removal of organic dyes with high efficiency: Kinetic and isotherm studies, Journal of Environmental Chemical Engineering. 8 (2020) 103780. https://doi.org/10.1016/j.jece.2020.103780.

[18] F. Lu, D. Astruc, Nanocatalysts and other nanomaterials for water remediation from organic pollutants, Coordination Chemistry Reviews. 408 (2020) 213180. https://doi.org/10.1016/j.ccr.2020.213180.

[19] Z. Jian, J. Xu, N. Yang, S. Han, X. Jiang, A perspective on diamond composites and their electrochemical applications, Current Opinion in Electrochemistry. 30 (2021) 100835. https://doi.org/10.1016/j.coelec.2021.100835.

[20] N. Yang, X. Jiang, Diamond Nanostructures and Nanoparticles: Electrochemical Properties and Applications, in: N. Yang, X. Jiang, D.-W. Pang (Eds.), Carbon Nanoparticles and Nanostructures, Springer International Publishing, Cham, 2016: pp. 299–330. https://doi.org/10.1007/978-3-319-28782-9_9.

[21] X. Duan, H. Sun, S. Wang, Metal-Free Carbocatalysis in Advanced Oxidation Reactions, Acc. Chem. Res. 51 (2018) 678–687. https://doi.org/10.1021/acs.accounts.7b00535.

[22] Y. Zhang, K.Y. Rhee, D. Hui, S.-J. Park, A critical review of nanodiamond based nanocomposites: Synthesis, properties and applications, Composites Part B: Engineering. 143 (2018) 19–27. https://doi.org/10.1016/j.compositesb.2018.01.028.

[23] B. Yang, H. Kang, Y.-J. Ko, H. Woo, G. Gim, J. Choi, J. Kim, K. Cho, E.-J. Kim, S.-G. Lee, H. Lee, J. Lee, Persulfate activation by nanodiamond-derived carbon onions: Effect of phase transformation of the inner diamond core on reaction kinetics and mechanisms, Applied Catalysis B: Environmental. 293 (2021) 120205. https://doi.org/10.1016/j.apcatb.2021.120205.

[24] H. Lee, H. Kim, S. Weon, W. Choi, Y.S. Hwang, J. Seo, C. Lee, J.-H. Kim, Activation of Persulfates by Graphitized Nanodiamonds for Removal of Organic Compounds, Environ. Sci. Technol. 50 (2016) 10134–10142. https://doi.org/10.1021/acs.est.6b02079.

[25] D. Banerjee, K.J. Sankaran, S. Deshmukh, M. Ficek, G. Bhattacharya, J. Ryl, D.M. Phase, M. Gupta, R. Bogdanowicz, I.-N. Lin, A. Kanjilal, K. Haenen, S.S. Roy, 3D Hierarchical Boron-Doped Diamond-Multilayered Graphene Nanowalls as an Efficient Supercapacitor Electrode, J. Phys. Chem. C. 123 (2019) 15458–15466. https://doi.org/10.1021/acs.jpcc.9b03628.

[26] M. Sobaszek, K. Siuzdak, J. Ryl, M. Sawczak, S. Gupta, S.B. Carrizosa, M. Ficek, B. Dec, K. Darowicki, R. Bogdanowicz, Diamond Phase (sp3-C) Rich Boron-Doped Carbon Nanowalls (sp2-C): Physicochemical and Electrochemical Properties, J. Phys. Chem. C. 121 (2017) 20821–20833. https://doi.org/10.1021/acs.jpcc.7b06365.

[27] H. Lee, C. Lee, J.-H. Kim, Response to Comment on "Activation of Persulfate by Graphitized Nanodiamonds for Removal of Organic Compounds," Environ. Sci. Technol. 51 (2017) 5353–5354. https://doi.org/10.1021/acs.est.7b01642.

[28] X. Duan, H. Sun, S. Wang, Comment on "Activation of Persulfate by Graphitized Nanodiamonds for Removal of Organic Compounds," Environ. Sci. Technol. 51 (2017) 5351–5352. https://doi.org/10.1021/acs.est.7b00399.

[29] P. Shao, J. Tian, F. Yang, X. Duan, S. Gao, W. Shi, X. Luo, F. Cui, S. Luo, S. Wang, Identification and Regulation of Active Sites on Nanodiamonds: Establishing a Highly Efficient Catalytic System for Oxidation of Organic Contaminants, Advanced Functional Materials. 28 (2018) 1705295. https://doi.org/10.1002/adfm.201705295.

[30] X. Duan, Z. Ao, H. Zhang, M. Saunders, H. Sun, Z. Shao, S. Wang, Nanodiamonds in sp2/sp3 configuration for radical to nonradical oxidation: Core-shell layer dependence, Applied Catalysis B: Environmental. 222 (2018) 176–181. https://doi.org/10.1016/j.apcatb.2017.10.007.

[31] X. Duan, Z. Ao, D. Li, H. Sun, L. Zhou, A. Suvorova, M. Saunders, G. Wang, S. Wang, Surface-tailored nanodiamonds as excellent metal-free catalysts for organic oxidation, Carbon. 103 (2016) 404–411. https://doi.org/10.1016/j.carbon.2016.03.034.

[32] S. Zhu, X. Li, J. Kang, X. Duan, S. Wang, Persulfate Activation on Crystallographic Manganese Oxides: Mechanism of Singlet Oxygen Evolution for Nonradical Selective Degradation of Aqueous Contaminants, Environ. Sci. Technol. 53 (2019) 307–315. https://doi.org/10.1021/acs.est.8b04669.

[33] D.T. Oyekunle, X. Zhou, A. Shahzad, Z. Chen, Review on carbonaceous materials as persulfate activators: structure–performance relationship, mechanism and future perspectives on water treatment, J. Mater. Chem. A. 9 (2021) 8012–8050. https://doi.org/10.1039/D1TA00033K.

[34] P. Shao, Y. Jing, X. Duan, H. Lin, L. Yang, W. Ren, F. Deng, B. Li, X. Luo, S. Wang, Revisiting the Graphitized Nanodiamond-Mediated Activation of Peroxymonosulfate: Singlet Oxygenation versus Electron Transfer, Environ. Sci. Technol. 55 (2021) 16078–16087. https://doi.org/10.1021/acs.est.1c02042.

[35] D. Guo, S. You, F. Li, Y. Liu, Engineering carbon nanocatalysts towards efficient degradation of emerging organic contaminants via persulfate activation: A review, Chinese Chemical Letters. 33 (2022) 1–10. https://doi.org/10.1016/j.cclet.2021.06.027.

[36] L.D. Dias, F.M.S. Rodrigues, M.J.F. Calvete, S.A.C. Carabineiro, M.D. Scherer, A.R.L. Caires, J.G. Buijnsters, J.L. Figueiredo, V.S. Bagnato, M.M. Pereira, Porphyrin–Nanodiamond Hybrid Materials—Active, Stable and Reusable Cyclohexene Oxidation Catalysts, Catalysts. 10 (2020) 1402. https://doi.org/10.3390/catal10121402.

[37] E.-T. Yun, G.-H. Moon, H. Lee, T.H. Jeon, C. Lee, W. Choi, J. Lee, Oxidation of organic pollutants by peroxymonosulfate activated with low-temperature-modified nanodiamonds: Understanding the reaction kinetics and mechanism, Applied Catalysis B: Environmental. 237 (2018) 432–441. https://doi.org/10.1016/j.apcatb.2018.04.067.

[38] K. Sato, M. Aoki, R. Noyori, A "Green" Route to Adipic Acid: Direct Oxidation of Cyclohexenes with 30 Percent Hydrogen Peroxide, Science. 281 (1998) 1646–1647. https://doi.org/10.1126/science.281.5383.1646.

[39] E. Brun, H.A. Girard, J.-C. Arnault, M. Mermoux, C. Sicard-Roselli, Hydrogen plasma treated nanodiamonds lead to an overproduction of hydroxyl radicals and solvated electrons in solution under ionizing radiation, Carbon. 162 (2020) 510–518. https://doi.org/10.1016/j.carbon.2020.02.063.

[40] X. Duan, Z. Ao, L. Zhou, H. Sun, G. Wang, S. Wang, Occurrence of radical and nonradical pathways from carbocatalysts for aqueous and nonaqueous catalytic oxidation, Applied Catalysis B: Environmental. 188 (2016) 98–105. https://doi.org/10.1016/j.apcatb.2016.01.059.

[41] F. Bernat-Quesada, C. Vallés-García, E. Montero-Lanzuela, A. López-Francés, B. Ferrer, H.G. Baldoví, S. Navalón, Hybrid sp2/sp3 nanodiamonds as heterogeneous metal-free ozonation catalysts in water, Applied Catalysis B: Environmental. 299 (2021) 120673. https://doi.org/10.1016/j.apcatb.2021.120673.

[42] Z. Jian, M. Heide, N. Yang, C. Engelhard, X. Jiang, Diamond fibers for efficient electrocatalytic degradation of environmental pollutants, Carbon. 175 (2021) 36–42. https://doi.org/10.1016/j.carbon.2020.12.066.

[43] M.A. Ajeel, R.I. Mahdi, M.K.T. Aroua, W. Abd Majid, Preparation and characterization of electrode from annealed nano-diamond particles with boric acid for anodic oxidation process, Electrochimica Acta. 362 (2020) 137221. https://doi.org/10.1016/j.electacta.2020.137221.

[44] H. Song, L. Yan, J. Jiang, J. Ma, Z. Zhang, J. Zhang, P. Liu, T. Yang, Electrochemical activation of persulfates at BDD anode: Radical or nonradical oxidation?, Water Research. 128 (2018) 393–401. https://doi.org/10.1016/j.watres.2017.10.018.

[45] M. Pierpaoli, M. Szopińska, B.K. Wilk, M. Sobaszek, A. Łuczkiewicz, R. Bogdanowicz, S. Fudala-Książek, Electrochemical oxidation of PFOA and PFOS in landfill leachates at low and highly boron-doped diamond electrodes, Journal of Hazardous Materials. 403 (2021) 123606. https://doi.org/10.1016/j.jhazmat.2020.123606.

[46] N. Yang, S. Yu, J. V. Macpherson, Y. Einaga, H. Zhao, G. Zhao, G. M. Swain, X. Jiang, Conductive diamond: synthesis, properties, and electrochemical applications, Chemical Society Reviews. 48 (2019) 157–204. https://doi.org/10.1039/C7CS00757D.

[47] S. Tago, T. Ochiai, S. Suzuki, M. Hayashi, T. Kondo, A. Fujishima, Flexible Boron-Doped Diamond (BDD) Electrodes for Plant Monitoring, Sensors. 17 (2017) 1638. https://doi.org/10.3390/s17071638.

[48] V. Srivastava, M. Suresh Kumar, P.V. Nidheesh, C.A. Martínez-Huitle, Electro catalytic generation of reactive species at diamond electrodes and applications in microbial inactivation, Current Opinion in Electrochemistry. 30 (2021) 100849. https://doi.org/10.1016/j.coelec.2021.100849.

[49] X. Du, M.A. Oturan, M. Zhou, N. Belkessa, P. Su, J. Cai, C. Trellu, E. Mousset, Nanostructured electrodes for electrocatalytic advanced oxidation processes: From materials preparation to mechanisms understanding and wastewater treatment applications, Applied Catalysis B: Environmental. 296 (2021) 120332. https://doi.org/10.1016/j.apcatb.2021.120332.

[50] Y. Liu, S. Chen, X. Quan, X. Fan, H. Zhao, Q. Zhao, H. Yu, Nitrogen-doped nanodiamond rod array electrode with superior performance for electroreductive debromination of polybrominated diphenyl ethers, Applied Catalysis B: Environmental. 154–155 (2014) 206–212. https://doi.org/10.1016/j.apcatb.2014.02.028.

[51] Y. Zhang, S. Yoshihara, T. Shirakashi, T. Kyomen, Electrochemical characteristics of boron-doped, undoped and nitrogen-doped diamond films, Diamond and Related Materials. 14 (2005) 213–219. https://doi.org/10.1016/j.diamond.2004.11.039.

[52] H. Ashassi-Sorkhabi, B. Rezaei-Moghadam, E. Asghari, Electrosynthesis of polypyrrole–nanodiamond composite film under ultrasound irradiation: Promotion for methanol electrooxidation by gold and Cu2O nanostructures, Journal of the Taiwan Institute of Chemical Engineers. 75 (2017) 263–270. https://doi.org/10.1016/j.jtice.2017.03.011.

[53] J. Henych, Š. Stehlík, K. Mazanec, J. Tolasz, J. Čermák, B. Rezek, A. Mattsson, L. Österlund, Reactive adsorption and photodegradation of soman and dimethyl methylphosphonate on TiO2/nanodiamond composites, Applied Catalysis B: Environmental. 259 (2019) 118097. https://doi.org/10.1016/j.apcatb.2019.118097.

[54] M. J. Sampaio, L. M. Pastrana-Martínez, A.M. T. Silva, J. G. Buijnsters, C. Han, C. G. Silva, S.A. C. Carabineiro, D. D. Dionysiou, J. L. Faria, Nanodiamond–TiO 2 composites for photocatalytic degradation of microcystin-LA in aqueous solutions under simulated solar light, RSC Advances. 5 (2015) 58363–58370. https://doi.org/10.1039/C5RA08812G.

[55] L.-X. Su, Q. Lou, C.-X. Shan, D.-L. Chen, J.-H. Zang, L.-J. Liu, Ag/Nanodiamond/g-C3N4 heterostructures with enhanced visible-light photocatalytic performance, Applied Surface Science. 525 (2020) 146576. https://doi.org/10.1016/j.apsusc.2020.146576.

[56] Z. Wang, F. Zhang, A. Ning, D. Lv, G. Jiang, A. Song, Nanosilver supported on inert nano-diamond as a direct plasmonic photocatalyst for degradation of methyl blue, Journal of Environmental Chemical Engineering. 9 (2021) 104912. https://doi.org/10.1016/j.jece.2020.104912.

[57] J. Liu, P. Wang, W. Qu, H. Li, L. Shi, D. Zhang, Nanodiamond-decorated ZnO catalysts with enhanced photocorrosion-resistance for photocatalytic degradation of gaseous toluene, Applied Catalysis B: Environmental. 257 (2019) 117880. https://doi.org/10.1016/j.apcatb.2019.117880.

[58] Y. Li, S. He, Z. Zhou, S. Zhou, S. Huang, A.G. Fane, C. Zheng, Y. Zhang, S. Zhao, Carboxylated Nanodiamond-Enhanced Photocatalytic Membranes with Improved Antifouling and Self-Cleaning Properties, Ind. Eng. Chem. Res. 59 (2020) 3538–3549. https://doi.org/10.1021/acs.iecr.9b06389.

[59] J. Beltz, A. Pfaff, I.M. Abdullahi, A. Cristea, V.N. Mochalin, N. Ercal, Effect of nanodiamond surface chemistry on adsorption and release of tiopronin, Diamond and Related Materials. 100 (2019) 107590. https://doi.org/10.1016/j.diamond.2019.107590.

[60] A.B. Çiğil, O.A. Urucu, M.V. Kahraman, Nanodiamond-containing polyethyleneimine hybrid materials for lead adsorption from aqueous media, Journal of Applied Polymer Science. 136 (2019) 48241. https://doi.org/10.1002/app.48241.

[61] Z. He, Q. Huang, L. Mao, H. Huang, M. Liu, J. Chen, F. Deng, N. Zhou, X. Zhang, Y. Wei, Direct surface modification of nanodiamonds with ionic copolymers for fast adsorptive removal of copper ions with high efficiency, Colloid and Interface Science Communications. 37 (2020) 100278. https://doi.org/10.1016/j.colcom.2020.100278.

[62] A. Tizchang, Y. Jafarzadeh, R. Yegani, E. Shokri, Polysulfone nanocomposite membrane embedded by silanized nanodiamond for removal of humic acid from water, Journal of Water and Environmental Nanotechnology. 4 (2019) 213–226. https://doi.org/10.22090/jwent.2019.03.004.

[63] H. Molavi, A. Shojaei, A. Pourghaderi, Rapid and tunable selective adsorption of dyes using thermally oxidized nanodiamond, Journal of Colloid and Interface Science. 524 (2018) 52–64. https://doi.org/10.1016/j.jcis.2018.03.088.

[64] A. Li, X. Yang, B. Yu, X. Cai, Immobilization of horseradish peroxidase on polyglycerol-functionalized magnetic Fe3O4/nanodiamond nanocomposites and its application in phenol biodegradation, Res Chem Intermed. 46 (2020) 101–118. https://doi.org/10.1007/s11164-019-03937-7.

[65] S.A. Ansari, Q. Husain, Potential applications of enzymes immobilized on/in nano materials: A review, Biotechnology Advances. 30 (2012) 512–523. https://doi.org/10.1016/j.biotechadv.2011.09.005.

[66] G. Yang, H. Huang, J. Chen, D. Gan, F. Deng, Q. Huang, Y. Wen, M. Liu, X. Zhang, Y. Wei, Preparation of ionic liquids functionalized nanodiamonds-based composites through the Michael addition reaction for efficient removal of environmental pollutants, Journal of Molecular Liquids. 296 (2019) 111874. https://doi.org/10.1016/j.molliq.2019.111874.

[67] A. Tizchang, Y. Jafarzadeh, R. Yegani, S. Khakpour, The effects of pristine and silanized nanodiamond on the performance of polysulfone membranes for wastewater treatment by MBR system, Journal of Environmental Chemical Engineering. 7 (2019) 103447. https://doi.org/10.1016/j.jece.2019.103447.

[68] A. Fernandes, P. Makoś, G. Boczkaj, Treatment of bitumen post oxidative effluents by sulfate radicals based advanced oxidation processes (S-AOPs) under alkaline pH conditions, Journal of Cleaner Production. 195 (2018) 374–384. https://doi.org/10.1016/j.jclepro.2018.05.207.

[69] J. Rodríguez-Chueca, E. Laski, C. García-Cañibano, M.J. Martín de Vidales, Á. Encinas, B. Kuch, J. Marugán, Micropollutants removal by full-scale UV-C/sulfate radical based Advanced Oxidation Processes, Science of The Total Environment. 630 (2018) 1216–1225. https://doi.org/10.1016/j.scitotenv.2018.02.279.

[70] L. Ismail, C. Ferronato, L. Fine, F. Jaber, J.-M. Chovelon, Elimination of sulfaclozine from water with SO4− radicals: Evaluation of different persulfate activation methods, Applied Catalysis B: Environmental. 201 (2017) 573–581. https://doi.org/10.1016/j.apcatb.2016.08.046.

[71] L. Carolina Espinoza, C. Candia-Onfray, J. Vidal, R. Salazar, Influence of the chemical nature of Boron-Doped diamond anodes on wastewater treatments, Current Opinion in Solid State and Materials Science. 25 (2021) 100963. https://doi.org/10.1016/j.cossms.2021.100963.

[72] A.V. Karim, P.V. Nidheesh, M.A. Oturan, Boron-doped diamond electrodes for the mineralization of organic pollutants in the real wastewater, Current Opinion in Electrochemistry. 30 (2021) 100855. https://doi.org/10.1016/j.coelec.2021.100855.

[73] A.S. Mora, S.T. McBeath, C.A. Cid, M.R. Hoffmann, N.J.D. Graham, Diamond electrode facilitated electrosynthesis of water and wastewater treatment oxidants, Current Opinion in Electrochemistry. 32 (2022) 100899. https://doi.org/10.1016/j.coelec.2021.100899.

[74] C.A. Martínez-Huitle, E. Brillas, A critical review over the electrochemical disinfection of bacteria in synthetic and real wastewaters using a boron-doped diamond anode, Current Opinion in Solid State and Materials Science. 25 (2021) 100926. https://doi.org/10.1016/j.cossms.2021.100926.

[75] C.P. Chardon, T. Matthée, R. Neuber, M. Fryda, C. Comninellis, Efficient Electrochemical Production of Peroxodicarbonate Applying DIACHEM® Diamond Electrodes, ChemistrySelect. 2 (2017) 1037–1040. https://doi.org/10.1002/slct.201601583.

[76] K. Wenderich, B.A.M. Nieuweweme, G. Mul, B.T. Mei, Selective Electrochemical Oxidation of H2O to H2O2 Using Boron-Doped Diamond: An Experimental and Techno-Economic Evaluation, ACS Sustainable Chem. Eng. 9 (2021) 7803–7812. https://doi.org/10.1021/acssuschemeng.1c01244.

[77] S.T. McBeath, D.P. Wilkinson, N.J.D. Graham, Application of boron-doped diamond electrodes for the anodic oxidation of pesticide micropollutants in a water treatment process: a critical review, Environ. Sci.: Water Res. Technol. 5 (2019) 2090–2107. https://doi.org/10.1039/C9EW00589G.

[78] C. Zhang, X. Chen, S.-H. Ho, Wastewater treatment nexus: Carbon nanomaterials towards potential aquatic ecotoxicity, Journal of Hazardous Materials. 417 (2021) 125959. https://doi.org/10.1016/j.jhazmat.2021.125959.